



## The African Regional Greenhouse Gases Budget (2010–2019)

Yolandi Ernst, Sally Archibald, Heiko Balzter, Frederic Chevallier, Philippe Ciais, Carlos Gonzalez Fischer, Benjamin Gaubert, Thomas Higginbottom, Steven Higgins, Shakirudeen Lawal, et al.

### ► To cite this version:

Yolandi Ernst, Sally Archibald, Heiko Balzter, Frederic Chevallier, Philippe Ciais, et al.. The African Regional Greenhouse Gases Budget (2010–2019). *Global Biogeochemical Cycles*, 2024, 38 (4), 10.1029/2023gb008016 . hal-04536918

**HAL Id: hal-04536918**

**<https://hal.science/hal-04536918>**

Submitted on 8 Apr 2024

**HAL** is a multi-disciplinary open access archive for the deposit and dissemination of scientific research documents, whether they are published or not. The documents may come from teaching and research institutions in France or abroad, or from public or private research centers.

L'archive ouverte pluridisciplinaire **HAL**, est destinée au dépôt et à la diffusion de documents scientifiques de niveau recherche, publiés ou non, émanant des établissements d'enseignement et de recherche français ou étrangers, des laboratoires publics ou privés.

# Global Biogeochemical Cycles<sup>\*</sup>

## RESEARCH ARTICLE

10.1029/2023GB008016

### Special Section:

Regional Carbon Cycle  
Assessment and Processes-2

### Key Points:

- Estimates of termite, herbivore, and fire emissions from novel methods
- Global woody biomass products constrained with high quality local data
- Africa a net source (approximately carbon neutral) between 2010 and 2019, sink capacity decreasing

### Supporting Information:

Supporting Information may be found in the online version of this article.

### Correspondence to:

Y. Ernst and S. Archibald,  
[yolandi.ernst@wits.ac.za](mailto:yolandi.ernst@wits.ac.za);  
[sally.archibald@wits.ac.za](mailto:sally.archibald@wits.ac.za)

### Citation:

Ernst, Y., Archibald, S., Balzter, H., Chevallier, F., Ciais, P., Fischer, C. G., et al. (2024). The African regional greenhouse gases budget (2010–2019). *Global Biogeochemical Cycles*, 38, e2023GB008016. <https://doi.org/10.1029/2023GB008016>

Received 23 OCT 2023

Accepted 22 FEB 2024

### Author Contributions:

















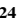




**Conceptualization:** Yolandi Ernst, Robert J. Scholes

**Formal analysis:** Yolandi Ernst, Sally Archibald, Heiko Balzter, Philippe Ciais, Benjamin Gaubert, Steven Higgins, Fabrice Lacroix, Ronny Lauerwald, Mauro Lourenco, Carola Martens, Anteneh G. Mengistu, Lutz Merbold, Mthokozisi Moyo, Hannah Nguyen, Michael O'Sullivan, Thais Rosan, Simon Scheiter, Stephen Stich, Torbern Tagesson, Hanqin Tian, Mengjia Wang, Joel S. Woon, Yong Zhou, Robert J. Scholes

© 2024. The Authors.

This is an open access article under the terms of the [Creative Commons Attribution-NonCommercial-NoDerivs License](#), which permits use and distribution in any medium, provided the original work is properly cited, the use is non-commercial and no modifications or adaptations are made.

## The African Regional Greenhouse Gases Budget (2010–2019)

Yolandi Ernst<sup>1</sup> , Sally Archibald<sup>2</sup>, Heiko Balzter<sup>3,4</sup> , Frederic Chevallier<sup>5</sup> , Philippe Ciais<sup>5</sup> , Carlos Gonzalez Fischer<sup>6</sup> , Benjamin Gaubert<sup>7</sup> , Thomas Higginbottom<sup>8</sup>, Steven Higgins<sup>9</sup>, Shakirudeen Lawal<sup>10</sup>, Fabrice Lacroix<sup>11,12</sup>, Ronny Lauerwald<sup>13</sup> , Mauro Lourenco<sup>2,14</sup> , Carola Martens<sup>15,16</sup>, Anteneh G. Mengistu<sup>17</sup>, Lutz Merbold<sup>18</sup> , Edward Mitchard<sup>19</sup> , Mthokozisi Moyo<sup>2</sup> , Hannah Nguyen<sup>20</sup>, Michael O'Sullivan<sup>21</sup>, Pedro Rodriguez-Veiga<sup>22,23</sup> , Thais Rosan<sup>24</sup> , Judith Rosentreter<sup>25</sup> , Casey Ryan<sup>26</sup> , Simon Scheiter<sup>15</sup> , Stephen Stich<sup>24</sup> , Nicola Stevens<sup>2,27</sup> , Torbern Tagesson<sup>28,29</sup>, Hanqin Tian<sup>30</sup> , Mengjia Wang<sup>31,32</sup>, Joel S. Woon<sup>33</sup>, Bo Zheng<sup>34,35</sup> , Yong Zhou<sup>36,37</sup> , and Robert J. Scholes<sup>1</sup>

<sup>1</sup>Global Change Institute, University of the Witwatersrand, Johannesburg, South Africa, <sup>2</sup>School of Animal, Plant and Environmental Sciences, University of the Witwatersrand, Johannesburg, South Africa, <sup>3</sup>Institute for Environmental Futures, School of Geography, Geology and the Environment, University of Leicester, Space Park Leicester, Leicester, UK, <sup>4</sup>National Centre for Earth Observation, University of Leicester, Space Park Leicester, Leicester, UK, <sup>5</sup>Laboratoire des Sciences du Climat et de l'Environnement, LSCE/IPSIL, CEA-CNRS-UVSQ, Université Paris-Saclay, Gif-sur-Yvette, France, <sup>6</sup>Department of Global Development, College of Agriculture and Life Sciences, Cornell University, Ithaca, NY, USA, <sup>7</sup>Atmospheric Chemistry Observations & Modeling Laboratory (ACOM), NSF National Center for Atmospheric Research (NSF NCAR), Boulder, CO, USA, <sup>8</sup>School of GeoSciences, University of Edinburgh, Edinburgh, UK, <sup>9</sup>Plant Ecology, University of Bayreuth, Bayreuth, Germany, <sup>10</sup>Department of Forestry and Environmental Resources, College of Natural Resources, North Carolina State University, Raleigh, NC, USA, <sup>11</sup>Climate and Environmental Physics, University of Bern, Bern, Switzerland, <sup>12</sup>Oeschger Centre for Climate Change Research (OCCR), University of Bern, Bern, Switzerland, <sup>13</sup>INRAE, AgroParisTech, UMR ECOSYS, Université Paris-Saclay, Palaiseau, France, <sup>14</sup>National Geographic Okavango Wilderness Project, Wild Bird Trust, Johannesburg, South Africa, <sup>15</sup>Senckenberg Biodiversity and Climate Research Centre (SBiK-F), Frankfurt am Main, Germany, <sup>16</sup>Institute of Physical Geography, Goethe University Frankfurt am Main, Frankfurt am Main, Germany, <sup>17</sup>Finnish Meteorological Institute, Helsinki, Finland, <sup>18</sup>Integrative Agroecology Group, Strategic Research Division Agroecology and Environment, Agroscope, Zurich, Switzerland, <sup>19</sup>School of GeoSciences, King's Buildings, University of Edinburgh, Edinburgh, UK, <sup>20</sup>Department of Geography, King's College London Strand, London, UK, <sup>21</sup>Faculty of Environment, Science and Economy, University of Exeter, Exeter, UK, <sup>22</sup>Sylvera Ltd, London, UK, <sup>23</sup>Centre for Landscape and Climate Research, School of Geography, Geology and the Environment, University of Leicester, Leicester, UK, <sup>24</sup>College of Life and Environmental Sciences, University of Exeter, Exeter, UK, <sup>25</sup>Faculty of Science and Engineering, Southern Cross University, Lismore, NSW, Australia, <sup>26</sup>School of GeoScience, University of Edinburgh, Edinburgh, UK, <sup>27</sup>Environmental Change Institute, School of Geography and the Environment, University of Oxford, Oxford, UK, <sup>28</sup>Department of Physical Geography and Ecosystem Science, Lund University, Lund, Sweden, <sup>29</sup>Department of Geosciences and Natural Resource Management, University of Copenhagen, Copenhagen, Denmark, <sup>30</sup>Center for Earth System Science and Global Sustainability, Schiller Institute for Integrated Science and Society, Department of Earth and Environmental Sciences, Boston College, Chestnut Hill, MA, USA, <sup>31</sup>School of Geoscience and Technology, Zhengzhou University, Zhengzhou, China, <sup>32</sup>INRAE, UMR1391 ISPA, Université de Bordeaux, Villenave d'Ornon, France, <sup>33</sup>School of Environmental Sciences, University of Liverpool, Liverpool, UK, <sup>34</sup>Department of Earth System Science, Tsinghua University, Beijing, China, <sup>35</sup>State Key Joint Laboratory of Environment Simulation and Pollution Control, School of Environment, Tsinghua University, Beijing, China, <sup>36</sup>Department of Wildland Resources, Utah State University, Logan, UT, USA, <sup>37</sup>Ecology Center, Utah State University, Logan, UT, USA

**Abstract** As part of the REgional Carbon Cycle Assessment and Processes Phase 2 (RECCAP2) project, we developed a comprehensive African Greenhouse gases (GHG) budget covering 2000 to 2019 (RECCAP1 and RECCAP2 time periods), and assessed uncertainties and trends over time. We compared bottom-up process-based models, data-driven remotely sensed products, and national GHG inventories with top-down atmospheric inversions, accounting also for lateral fluxes. We incorporated emission estimates derived from novel methodologies for termites, herbivores, and fire, which are particularly important in Africa. We further constrained global woody biomass change products with high-quality regional observations. During the RECCAP2 period, Africa's carbon sink capacity is decreasing, with net ecosystem exchange switching from a small sink of  $-0.61 \pm 0.58$  PgC yr<sup>-1</sup> in RECCAP1 to a small source in RECCAP2 at  $0.16$  ( $-0.52/1.36$ ) PgC yr<sup>-1</sup>. Net CO<sub>2</sub> emissions estimated from bottom-up approaches were  $1.6$  ( $-0.9/5.8$ ) PgCO<sub>2</sub> yr<sup>-1</sup>, net CH<sub>4</sub> were  $77$  ( $56.4/93.9$ ) TgCH<sub>4</sub> yr<sup>-1</sup> and net N<sub>2</sub>O were  $2.9$  ( $1.4/4.9$ ) TgN<sub>2</sub>O yr<sup>-1</sup>. Top-down atmospheric inversions showed similar trends. Land Use Change emissions increased, representing one of the largest contributions at

**Investigation:** Yolandi Ernst,  
Sally Archibald, Carlos Gonzalez Fischer  
**Methodology:** Yolandi Ernst,  
Sally Archibald, Heiko Balzter,  
Pedro Rodríguez-Veiga

**Project administration:** Yolandi Ernst,  
Sally Archibald, Robert J. Scholes

**Resources:** Heiko Balzter,  
Frederic Chevallier, Philippe Ciais, Carlos  
Gonzalez Fischer, Thomas Higginbottom,  
Steven Higgins, Shakirudeen Lawal,  
Fabrice Lacroix, Ronny Lauerwald,  
Mauro Lourenco, Carola Martens,  
Lutz Merbold, Edward Mitchard,  
Mthokozisi Moyo, Hannah Nguyen,  
Michael O'Sullivan, Pedro Rodríguez-  
Veiga, Thais Rosan, Judith Rosentreter,  
Casey Ryan, Simon Scheiter,  
Stephen Sitch, Nicola Stevens,  
Torbern Tagesson, Hanqin Tian,  
Mengjia Wang, Joel S. Woon, Bo Zheng,  
Yong Zhou

**Writing – original draft:** Yolandi Ernst,  
Sally Archibald, Frederic Chevallier,  
Philippe Ciais, Benjamin Gaubert,  
Thomas Higginbottom, Steven Higgins,  
Shakirudeen Lawal, Fabrice Lacroix,  
Ronny Lauerwald, Mauro Lourenco,  
Carola Martens, Anteneh G. Mengistu,  
Lutz Merbold, Edward Mitchard,  
Mthokozisi Moyo, Hannah Nguyen,  
Michael O'Sullivan, Thais Rosan,  
Judith Rosentreter, Casey Ryan,  
Simon Scheiter, Stephen Sitch,  
Nicola Stevens, Torbern Tagesson,  
Hanqin Tian, Mengjia Wang, Joel  
S. Woon, Bo Zheng, Yong Zhou, Robert  
J. Scholes

**Writing – review & editing:**  
Yolandi Ernst, Sally Archibald,  
Heiko Balzter, Pedro Rodríguez-Veiga

1.7 (0.8/2.7) PgCO<sub>2</sub>eq yr<sup>-1</sup> to the African GHG budget and almost similar to emissions from fossil fuels at 1.74 (1.53/1.96) PgCO<sub>2</sub>eq yr<sup>-1</sup>, which also increased from RECCAP1. Additionally, wildfire emissions decreased, while fuelwood burning increased. For most component fluxes, uncertainty is large, highlighting the need for increased efforts to address Africa-specific data gaps. However, for RECCAP2, we improved our overall understanding of many of the important components of the African GHG budget that will assist to inform climate policy and action.

**Plain Language Summary** We developed a comprehensive greenhouse gases (GHG) budget for Africa as part of the REgional Carbon Cycle Assessment and Processes Phase 2 (RECCAP2) project over the 2010–2019 period. We used global and local data sets and innovative methods to estimate the different components of the budget. Our estimates show that wildfire emissions decreased; termite emissions may be less than previously expected and emissions from large mammals are increasing. We also used data from new satellite technology to estimate carbon that is stored in above-ground biomass in Africa. With increasing land use change and fossil fuel usage in Africa, the net bottom-up GHG estimate shows that Africa is a source at 4.5 (–3.3/14.1) PgCO<sub>2</sub>eq yr<sup>-1</sup>, with the top-down atmospheric inversion estimate smaller at 3.98 (3.13/4.85) PgCO<sub>2</sub>eq yr<sup>-1</sup>. However, our estimates continue to have large uncertainties owing to the differences between data sets and methods. It is therefore essential to increase efforts to expand the availability of high quality local data. Nevertheless, our work improved our understanding of all the components of the African GHG budget and will help to inform climate policy and action.

## 1. Introduction

Africa's role in the global greenhouse gases (GHG) cycles is of great interest due both to the large landmass covered by the continent, and the potential for rapid change in coming decades as the human population increases and land use patterns continue to evolve. Africa contains some of the largest tracts of untransformed land in the world, although it is often heavily utilized for grazing, fuelwood and other natural resources. With a current population of about 1.4 billion, set to increase to over 2 billion by 2040 (United Nations Urban Settlement Programme, 2019), it is expected that large areas of land will be converted for agricultural production to feed this increasingly urbanized community and to increase country-level GDP. Concurrently, there is massive interest in using African landscapes to store carbon and offset global carbon emissions (Armani, 2022). It is therefore imperative to develop reliable data on key carbon-cycle processes and GHG emissions to quantify the net effect of these competing trends.

Previous accounting efforts of the African GHG budget estimated the continent as a net biospheric sink but highlighted the large uncertainty associated with an inadequate observation network (Bombelli et al., 2009; Ciais et al., 2011; Valentini et al., 2014; Williams et al., 2007). Moreover, African savannas and woodlands, with seasonal rainfall, frequent fire and large populations of native and introduced herbivores, play a unique and significant role in the inter-annual variability of the continent's GHG fluxes that further contribute to uncertainty in estimates (Bombelli et al., 2009; Valentini et al., 2014).

Modeling studies indicate the risk for rapid and irreversible changes in vegetation cover in response to changing climates and CO<sub>2</sub> fertilization (e.g., greening in northern ecosystems and browning in tropical biomes) (Winkler et al., 2021). Field observations further demonstrate both extensive woody thickening as well as areas of reduced productivity in recent years (Stevens et al., 2016). Since the last continental-scale GHG budget for the 1985–2009 period (Valentini et al., 2014), we have seen improved estimations of fire (Andela et al., 2017; Hantson et al., 2016; Lasslop et al., 2020) and herbivore emissions (Hempson et al., 2017; Pachzelt et al., 2015) and better representation of African landscapes and functional types in Dynamic Global Vegetation Models (DGVMs) (e.g., aDGVM—Scheiter & Higgins, 2009). Estimates for other GHG budget components such as inland waters (Borges et al., 2015; Borges, Deirmendjian, Bouillon, Okello, et al., 2022; Lauerwald et al., 2023a) and geological fluxes (Etiopie et al., 2019; Lacroix et al., 2020) are also better represented.

The current synthesis of the GHG budget of Africa aims to integrate the most contemporary modeling and observational data sets to present a comprehensive and up to date summary of the key sources and sinks of carbon,

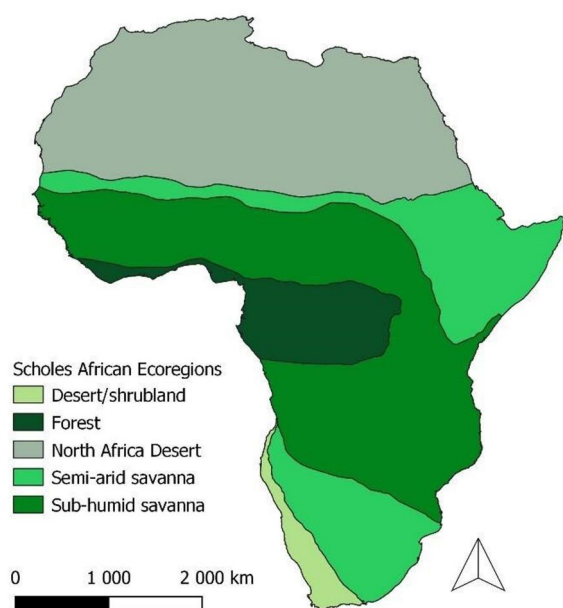


**Figure 1.** The Scholes African Ecoregions Map (Ernst & Scholes, 2023) was delineated by regrouping and smoothing the vegetation classification of the UNESCO/AETFAT/UNSO (White's) Vegetation Map of Africa (White, 1983) in accordance with the delineations of the distributions of Mean Annual Precipitation-determined ("stable") and Disturbance-determined ("unstable") savannas in Africa by Sankaran et al. (2005).

CO<sub>2</sub>, CH<sub>4</sub>, and N<sub>2</sub>O greenhouse gases and their associated uncertainties from 2010 to 2019. Where possible, analyses that include the 1985–2009 period are presented for comparison. Due to the limitations imposed by the availability of some data sets, some estimates may represent alternative dates for the RECCAP1 (1985–2009) and RECCAP2 period (2010–2019) but reference periods are defined where necessary.

As part of the Regional Carbon Cycle Assessment and Processes Phase 2 (RECCAP2, <https://www.globalcarbonproject.org/reccap/>) initiative of the Global Carbon Project (<https://www.globalcarbonproject.org/index.htm>), this paper addresses the policy-relevant objectives of RECCAP2 through a comprehensive overview of improved estimates of CO<sub>2</sub>, CH<sub>4</sub>, and N<sub>2</sub>O fluxes and variability. In the following sections, we report the methodology and results for various component fluxes and uncertainties for Africa as a whole and for five ecoregions, delineated for interpretive purposes (Figure 1). The structure of the paper includes a section on carbon stocks represented by aboveground (Section 2.1.1) and below-ground (Section 2.1.2) biomass estimates, after which we report on the component fluxes estimated from various bottom-up methods. These broadly include gross and net primary production estimates (Section 2.2); fire, large mammals and termites as fluxes of special importance to Africa (Section 2.3); fluxes from geological, aquatic and coastal systems (Section 2.4); trade fluxes (Section 2.5); and anthropogenic emissions with special focus on fossil fuel emissions (Section 2.6). In Section 2.7, we present the top-down atmospheric inversion model estimates for CO<sub>2</sub>, CH<sub>4</sub>, and N<sub>2</sub>O, followed by a synthesis (Section 3) of all the estimates provided in the preceding sections. Our approach follows the guidelines by Ciais et al. (2022).

### 1.1. Drivers of Change in the African Carbon Cycle

Together with increasing atmospheric CO<sub>2</sub>, changing climates and land use all impact carbon-cycle processes. African climates have warmed significantly over the last several decades (Engelbrecht et al., 2015), more so in the arid and semi-arid regions and particularly in East Africa. Rainfall has increased on average across all regions (Alahacoon et al., 2022) and variability between years is high and probably increasing. Consequently, aridity trends (as indexed by P/PET) are not uniform, with aridity increasing in East and Southern Africa, and decreasing in West Africa (Lickley & Solomon, 2018). Cropland area has increased, and over the two RECCAP periods Africa gained  $7.15 \pm 3.39 \times 10^5$  km<sup>2</sup> new cropland area, and lost  $1.83 \pm 1.94 \times 10^5$  km<sup>2</sup>, resulting in a net increase of  $5.32 \pm 3.94 \times 10^5$  km<sup>2</sup> from 2000 to 2019 (Potapov et al., 2022). Currently  $20.83 \pm 4.74 \times 10^5$  km<sup>2</sup> (or ~17%) of the global cropland area occurs in Africa, but mapping products disagree on whether cropland expansion has slowed in the last decade (see Text S1, Figures S1 and S2, Tables S1 and S2 in Supporting Information S1 for changes estimated by different products). Land use trends are discussed further in Section 2.2.2 on the TRENDY results. We summarize information on changing livestock numbers in Section 2.3.2 and above-ground biomass in Section 2.1.1.

## 2. African GHG Component Estimates

### 2.1. Biomass

#### 2.1.1. Aboveground Biomass Change

Since the RECCAP1 period, novel L-VOD passive microwave data (Diouf et al., 2015) and LiDAR-based biomass data (Potapov et al., 2021) have become available. These data have the potential to provide more comprehensive information on AGB changes than estimates derived from changes in land cover as they measure AGB change within the land cover classes. They therefore account both for losses due to degradation and natural disturbance as well as gains from regrowing vegetation and environmental drivers such as CO<sub>2</sub>-fertilization. These within-land cover changes are important for Africa as land cover conversion is estimated to account for only about 25% of the AGB change on the continent (X. Feng et al., 2021; McNicol et al., 2018). However,

**Table 1**

*Estimated Net Aboveground Biomass Annual Change 2010–2017 (in Tg Cyr<sup>-1</sup>) for Africa and Its Ecoregions*

Region	1985–2009	2010–2017			
	Valentini et al. (2014)	CCI	NCEO	L-VOD (Brandt et al., 2018)	X-VOD (M. Wang et al., 2021)
NH Desert		0.1	−1.4	−5.9	−3.0
Forest		44.8	−80.2	−20.8	−147.4
Sub-humid savanna		−118.6	−63.0	36.2	−92.1
Semi-arid savanna		−17.9	−7.5	−71.3	−62.6
Desert/shrubland		−0.3	−0.2	−10.0	−4.8
Miombo Ecoregion		−98.0	−22.0	−1.0	17.0
Africa	−234 to −72	−92.0	−152.3	−71.9	−309.9

*Note.* Positive values are fluxes into the land-surface (sink); negative values represent loss from the living biomass pool (predominantly into the atmosphere as a source, rather than into the soil). Products ordered from global (left) to regional (right) calibrations. The Miombo Ecoregion was added to include the locally calibrated and developed (McNicol et al., 2018) product and because it is a region of rapid change.

although many papers reporting changes in AGB in Africa have been published within the 1985–2019 period, there is no agreement on the regional trends or magnitude of the changes (Text S2 in Supporting Information S1). These disagreements in AGB change estimates are largely due to the varied methods used, which include bookkeeping models, LiDAR-derived products, and various microwave-derived products. However, differences in the observation time periods might also add to the uncertainty due to large inter-annual variation in AGB.

For RECCAP2, we compared five microwave- and VOD-derived AGB change estimates from 2010 to 2017, three of which have been developed and calibrated specifically for Africa. The L-VOD product (Brandt et al., 2018) was calibrated against the Baccini et al. (2012) LiDAR-derived AGB. The X-VOD product (M. Wang et al., 2021) was retrieved from the AMSR2/AMSR-E brightness temperature observations at the X-band, with Saatchi et al. (2011) AGB (LiDAR-derived), (Bouvet et al., 2018) AGB (SAR-derived), GlobBiomass (SAR-derived AGB) and ESA-CCI AGB (SAR-derived AGB) as the calibration references. The National Center for Earth Observation (NCEO) product (Rodríguez-Veiga & Balzter, 2021; Rodríguez-Veiga et al., 2017) uses GEDI canopy-height data and L-band SAR to produce a canopy-height model calibrated against LiDAR-derived biomass data. The global ESA-CCI Biomass product (Santoro et al., 2021) uses both C- and L-band RADAR to estimate growing stock volume, and converts this to AGB using allometric equations from published wood density and biomass expansion data. The updated McNicol et al. (2018) product for southern Africa is focused on accurately estimating changes in non-forest African ecosystems (i.e., in contrast to L-VOD which is also sensitive to high-biomass regions), and trains its product with in situ biomass measurements. All products have potential artifacts from soil moisture and range in spatial resolution from 25 km (Brandt LVOD) to 25 m (McNicol product). More details on the products are available in Table S3 in Supporting Information S1.

For each product, we calculated the annual change as  $(AGB_{2017} - AGB_{2010})/7$ . As 2017 was the end of a severe multi-year drought in southern Africa (Blamey et al., 2018), the trends might not be reliable, but it is the first time that so many different products have been compared over the same period and regions.

All the products estimate net AGB losses at the scale of Africa, ranging from  $-71.9$  to  $-309.9$  Tg Cyr<sup>-1</sup>, but there was no consistency in predicted trends across biome classes or regions (Table 1, Figure 2). For example, the ESA-CCI biomass product predicted biomass gains of 44 Tg Cyr<sup>-1</sup> in forest but losses of  $-118$  TCyr<sup>-1</sup> in sub-humid savannas, and the Brandt L-VOD product showed the opposite trend (forest loss:  $-20.8$  Tg Cyr<sup>-1</sup>, sub-humid savanna gains: 36.6 Tg Cyr<sup>-1</sup>). Generally, these estimates are within the range reported by Valentini et al. (2014), but the uncertainty remains high for RECCAP2. Global RADAR and VOD products are currently unlikely to represent the dynamics of African woodlands accurately because they often lack African calibration data, and potentially require locally defined algorithms to represent the lower-biomass dynamics of African woodlands.



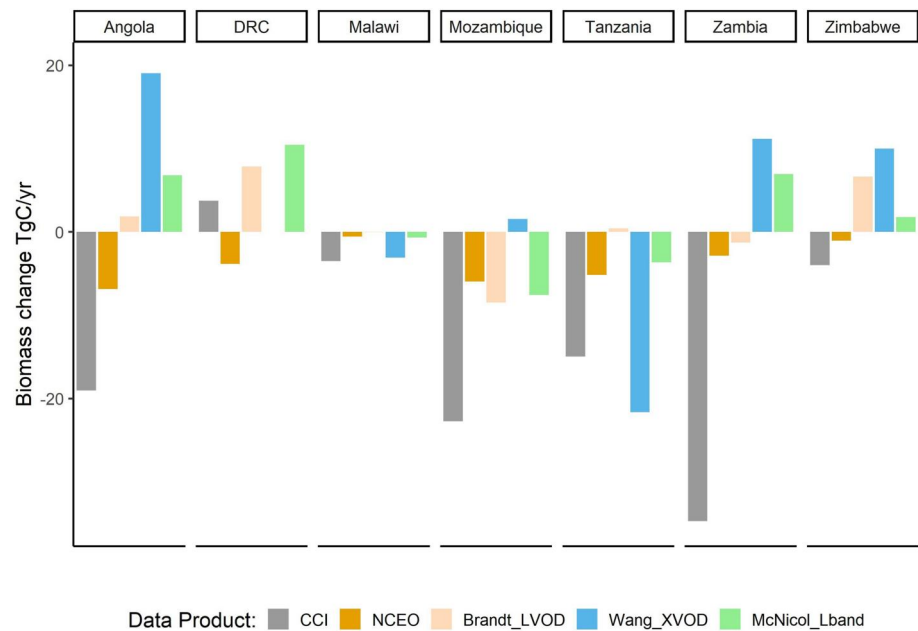


**Figure 2.** Change in aboveground biomass across seven countries in southern Africa for the period 2010–2017 as reported by five different RADAR-derived data products. Positive values are fluxes into the land-surface (sink); negative values represent loss from the living biomass pool (predominantly into the atmosphere as a source, rather than into the soil). There is no clarity on the trends between or within countries, but regionally and locally calibrated products report more sink capacity than globally calibrated products overall.

### 2.1.2. Belowground Carbon and Biomass

Since the previous synthesis of the African GHG budget, soil organic carbon (SOC) estimates (Table 2) have improved with the ISRIC (International Soil Reference and Information Center) producing soil property maps for the continent at 250 m resolution (Hengl et al., 2015, 2017a). These SoilGrids data (Hengl et al., 2017b) are interpolated from a network of several thousand soil cores and several hundred thousand surface samples, and estimate the SOC of Africa to be 87.7 PgC. Below-ground biomass carbon is poorly constrained and predicted from published root:shoot estimates. Recent quantification of biomass carbon in African grasslands (Gomes et al., 2021) indicates substantial below-ground stocks that are not accurately represented in existing continental-scale studies and are therefore likely to be under-estimates. These maps also still do not accurately map or account for peatlands, which are estimated to contain significant stores of carbon (Joosten, 2009). Currently, peat stocks are estimated at 36.9 PgC (UNEP, 2022), which is ~3 times higher than previous estimates of ~11 PgC due to new reserves found in the Congo basin (Dargie et al., 2017), and novel peat mapping methods (Lourenco et al., 2022).

**Table 2**  
Soil Organic Carbon, Peat Carbon Stocks, and Estimated Peat Loss Rates for Africa Per Ecoregion

Ecoregion	SOC (Pg) from SoilGrids	Peat carbon (Pg)			Valentini et al. (2014) <sup>a</sup>	aDGVM <sup>b</sup> 2009–2019		
	Total	Joosten (2009)	UNEP (2022)	Loss rate (PgC yr <sup>-1</sup> )	Total below-ground C	SOC	Biomass C	Total belowground C
NA Desert	3.7	2.1				4.33	0.67	5
Forest	15.7	3.6				13.29	3.92	17.21
Desert/shrubland	1.0	0.0				1.03	0.15	1.18
Sub-humid savanna	46.9	4.0				40.98	12.91	53.89
Semi-arid savanna	20.3	1.1				17.15	4.42	21.57
Total	87.7	10.8	36.9	0.013	167 (87–259)	76.77	22.08	98.85

<sup>a</sup>Valentini et al. (2014) model average—including biomass carbon. <sup>b</sup>aDGVM is a dynamic vegetation model developed for African ecosystems, see Section 2.3.3.

**Table 3**

*The Gross Primary Productivity Mean, Trend, and Inter-Annual Variability ( $\pm$  One Standard Deviation of Inter-Annual Variability  $\pm$  Model Variability) From Seven Global Earth Observation Products for Africa and Its Ecoregions for the 1985–2015 Periods*

Region	Mean GPP (Pg C yr <sup>-1</sup> )	Trend GPP (TgC yr <sup>-2</sup> )	Contributions (%) of Africa to global GPP budget/Ecoregions to Africa GPP budget		
			Mean	IAV*	Trend*
Africa (22.3% of global surface)	23.50 $\pm$ 0.41 $\pm$ 2.48	28.6 $\pm$ 6.47 $\pm$ 33.69	20.2 $\pm$ 0.4 $\pm$ 1.8	6.7 $\pm$ 1.1 $\pm$ 3.7	15.9 $\pm$ 3.6 $\pm$ 14.3
NA Desert (34.7% of Africa)	0.31 $\pm$ 0.02 $\pm$ 0.14	0.79 $\pm$ 0.41 $\pm$ 1.01	1.29 $\pm$ 0.1 $\pm$ 0.6	6.9 $\pm$ 0.4 $\pm$ 3.7	2.7 $\pm$ 1.4 $\pm$ 4.0
Forests (8.2% of Africa)	5.98 $\pm$ 0.06 $\pm$ 0.49	2.33 $\pm$ 1.05 $\pm$ 5.57	24.7 $\pm$ 0.2 $\pm$ 4.0	36.4 $\pm$ 1.2 $\pm$ 7.9	8.1 $\pm$ 3.7 $\pm$ 17.5
Desert/Shrubland (2.4% of Africa)	0.13 $\pm$ 0.01 $\pm$ 0.06	0.66 $\pm$ 0.15 $\pm$ 0.37	0.5 $\pm$ 0.0 $\pm$ 0.28	4.6 $\pm$ 0.1 $\pm$ 1.4	2.3 $\pm$ 0.5 $\pm$ 0.7
Sub-humid savanna (34.0% of Africa)	13.16 $\pm$ 0.23 $\pm$ 2.38	14.48 $\pm$ 3.73 $\pm$ 20.52	54.2 $\pm$ 0.9 $\pm$ 4.5	48.6 $\pm$ 4.7 $\pm$ 7.9	50.2 $\pm$ 12.9 $\pm$ 25.3
Semi-arid savanna (20.7% of Africa)	3.21 $\pm$ 0.15 $\pm$ 0.31	10.59 $\pm$ 2.47 $\pm$ 7.00	13.2 $\pm$ 0.6 $\pm$ 0.2	3.4 $\pm$ 2.3 $\pm$ 7.7	36.7 $\pm$ 8.6 $\pm$ 12.9

Peat loss, largely to the atmosphere, is estimated to be  $\sim 0.013$  PgC yr<sup>-1</sup> (Joosten, 2009) and is increasing. Below-ground stocks modeled from DGVMs varied from 87.5 to 259.5 PgC in the previous RECCAP period (Valentini et al., 2014). For the RECCAP2 period, aDGVM, a dynamic vegetation model developed for African ecosystems (Scheiter & Higgins, 2009, see also Section 2.2.3), estimates total stocks to be 98.9 PgC, of which SOC is 76.8 Pg and belowground biomass carbon 22.1 Pg. The TRENDY models show a mean SOC of  $148 \pm 60$  Pg and all but three show an increasing trend.

## 2.2. Gross and Net Primary Production Estimates

### 2.2.1. Satellite Observation Constrained Gross Primary Productivity Models

We used seven Earth observation based global scale vegetation gross primary productivity (GPP) data sets collected by Tagesson et al. (2021) for estimating Africa's GPP budgets 1985–2015. The contribution of Africa to the mean, trend, and inter-annual variability in the global scale GPP was estimated following Ahlström et al. (2015). The products with their spatial and temporal resolutions and estimates are listed in Table S4 in Supporting Information S1 and described in Tagesson et al. (2017). The average GPP budget for Africa over 1985–2015 was  $23.50 \pm 0.41$  ( $\pm$  one standard deviation of inter-annual variability)  $\pm 2.48$  PgC yr<sup>-1</sup> ( $\pm$  one standard deviation of model variability) (Table 3), which represents about 20% of the annual global GPP. This is relatively close to the 22.3% share Africa has of the global terrestrial surface area. Satellite observations indicate that the GPP is increasing by  $28.60 \pm 6.47 \pm 33.69$  TgC yr<sup>-1</sup>, over the 1985–2015 period (about 18.2% of the global trend), but the share of Africa in the inter-annual variability in the global GPP budgets was relatively low ( $6.77 \pm 1.13 \pm 3.74\%$ ).

Sub-humid savannas and forests were the main contributors to African GPP, contributing more than 50% and  $\sim 25\%$ , respectively (Table 3). Sub-humid savannas drove both the increasing trends and the inter-annual variability in GPP, with forest GPP being more stable with less strong trends. Semi-arid savannas, which contributed relatively little ( $3.21 \pm 0.15 \pm 0.31$  PgC yr<sup>-1</sup>) to the mean African GPP budgets, contributed substantially to the GPP trends (about a quarter of the GPP increases occurred in semi-arid savannas). Semi-arid regions in Africa are steadily becoming encroached with woody vegetation (Venter et al., 2018) and are important in terms of their inter-annual variability (Ahlström et al., 2015). The NA Desert and Desert/Shrubland regions have a very low share (about 1%) of the African GPP budget (Table 3). However, significant NA Desert trends and inter-annual variability (Table 3) indicate considerable changes in the vegetation cover during recent decades likely driven by CO<sub>2</sub> fertilization (Song et al., 2018).

The GPP of Africa increased over the period 1985–2015, but the increase slowed down in the last decade (Table 3). This could be caused by the strong drought in southern Africa at the end of the study period in 2015 (Blamey et al., 2018). Other reasons for a slowing down of the GPP trends could be a decrease in the degree to which CO<sub>2</sub> is upregulating photosynthesis (fertilization effect) (S. Wang et al., 2020), enhanced constraints from water supply, nutrient limitation, and land cover change (X. Feng et al., 2021; Peñuelas et al., 2013; Piao et al., 2020; Yuan et al., 2019). Still, Africa's contribution to the global GPP budgets are similar for both the RECCAP study periods: forest GPP contribution decreased slightly between RECCAP1 and RECCAP2, with

**Table 4***Regional Carbon Fluxes (Pg C yr<sup>-1</sup>) Decomposed Into the Three Main Drivers: Climate Change (CLIM), CO<sub>2</sub> Fertilization (CO<sub>2</sub>), and Land Use Change (LUC) Over the Last Four Decades*

Region	Forcing	Net ecosystem exchange (NEE PgC yr <sup>-1</sup> )			
		1980s	1990s	2000s	2010s
Africa	CLIM	0.33 ± 0.21	0.16 ± 0.12	0.21 ± 0.13	0.00 ± 0.15
	CO <sub>2</sub>	−0.41 ± 0.17	−0.39 ± 0.18	−0.56 ± 0.21	−0.55 ± 0.24
	LUC	0.18 ± 0.12	0.22 ± 0.13	0.28 ± 0.1	0.46 ± 0.15
	NET	0.10 ± 0.19	−0.01 ± 0.20	−0.07 ± 0.21	−0.09 ± 0.24
North Africa Desert	CLIM	0.01 ± 0.02	−0.00 ± 0.01	0.01 ± 0.00	−0.00 ± 0.02
	CO <sub>2</sub>	−0.01 ± 0.01	−0.01 ± 0.00	−0.01 ± 0.01	−0.01 ± 0.01
	LUC	−0.00 ± 0.01	−0.00 ± 0.01	−0.00 ± 0.01	−0.00 ± 0.01
	NET	0.01 ± 0.01	−0.00 ± 0.01	−0.01 ± 0.01	−0.01 ± 0.02
Forest	CLIM	0.03 ± 0.03	0.02 ± 0.03	0.03 ± 0.03	0.02 ± 0.02
	CO <sub>2</sub>	−0.11 ± 0.04	−0.13 ± 0.05	−0.15 ± 0.05	−0.17 ± 0.07
	LUC	0.04 ± 0.02	0.05 ± 0.03	0.05 ± 0.03	0.07 ± 0.04
	NET	−0.04 ± 0.04	−0.06 ± 0.05	−0.07 ± 0.04	−0.08 ± 0.06
Sub-humid savanna	CLIM	0.18 ± 0.14	0.11 ± 0.09	0.13 ± 0.09	0.01 ± 0.08
	CO <sub>2</sub>	−0.22 ± 0.13	−0.21 ± 0.13	−0.30 ± 0.17	−0.30 ± 0.17
	LUC	0.12 ± 0.08	0.15 ± 0.08	0.20 ± 0.07	0.33 ± 0.12
	NET	0.09 ± 0.13	0.05 ± 0.14	0.03 ± 0.14	0.04 ± 0.17
Semi-arid savanna	CLIM	0.00 ± 0.00	0.00 ± 0.00	0.00 ± 0.00	0.01 ± 0.00
	CO <sub>2</sub>	0.00 ± 0.00	0.00 ± 0.00	0.00 ± 0.00	0.00 ± 0.00
	LUC	0.00 ± 0.00	0.00 ± 0.00	0.00 ± 0.00	0.00 ± 0.00
	NET	0.00 ± 0.00	0.00 ± 0.00	0.00 ± 0.00	0.00 ± 0.00
Desert/Shrubland	CLIM	0.10 ± 0.08	0.03 ± 0.04	0.04 ± 0.02	0.03 ± 0.06
	CO <sub>2</sub>	−0.07 ± 0.03	−0.04 ± 0.03	−0.10 ± 0.03	−0.07 ± 0.04
	LUC	0.02 ± 0.02	0.02 ± 0.03	0.03 ± 0.02	0.05 ± 0.04
	NET	0.04 ± 0.06	0.01 ± 0.03	−0.02 ± 0.05	−0.04 ± 0.05

*Note.* Positive values represent fluxes out (source) of the biosphere and negative values, fluxes in (sinks).

increases in semi-arid savanna compensating for this. The semi-arid savanna also has an increasing GPP trend over 1985–2015 compared to forests, explaining their larger share during the RECCAP2 period.

### 2.2.2. Ecosystem Model Ensembles Including LUC: Trends in the Land Carbon Fluxes (TRENDY)

Outputs from an ensemble of 17 DGVMs from the TRENDY v.9 model suite were forced with observed changes in climate, CO<sub>2</sub> and nitrogen deposition, and Land Use Change (LUC) (Land Use Land Cover Change HYDE3.2 within LUH2-GCB) over the period 1985 to 2019 (Friedlingstein et al., 2020a) (Table 4).

We estimated changes in the African regional carbon fluxes and sinks and calculated their attribution to the underlying environmental drivers and the different ecoregions (Figure 3). Between 2000 and 2019, there were widespread but subtle losses due to climate change and variability (Figure 3c). The models also show a strong tropical forest uptake response driven by enhanced atmospheric CO<sub>2</sub> concentrations (Figure 3b), while LUC losses were concentrated in East and West Africa (Figure 3d). These large opposing fluxes result in Africa acting as a net sink between 2000 and 2019 (Figure 3a), but there are still large uncertainties around the magnitude of the estimates.

The model ensemble shows that losses due to LUC in Africa have increased over time (from 0.18 to 0.46 PgC yr<sup>-1</sup>) at a similar rate but in the opposite direction than the CO<sub>2</sub> fertilization sink increase (from −0.41 to −0.55 PgC yr<sup>-1</sup>, Table 4). This estimate for the RECCAP2 period is within the range of LUC emission estimates for Africa reported from bookkeeping models: BLUE (Hansis et al., 2015): 0.57 ± 0.06 PgC yr<sup>-1</sup> and HN2017



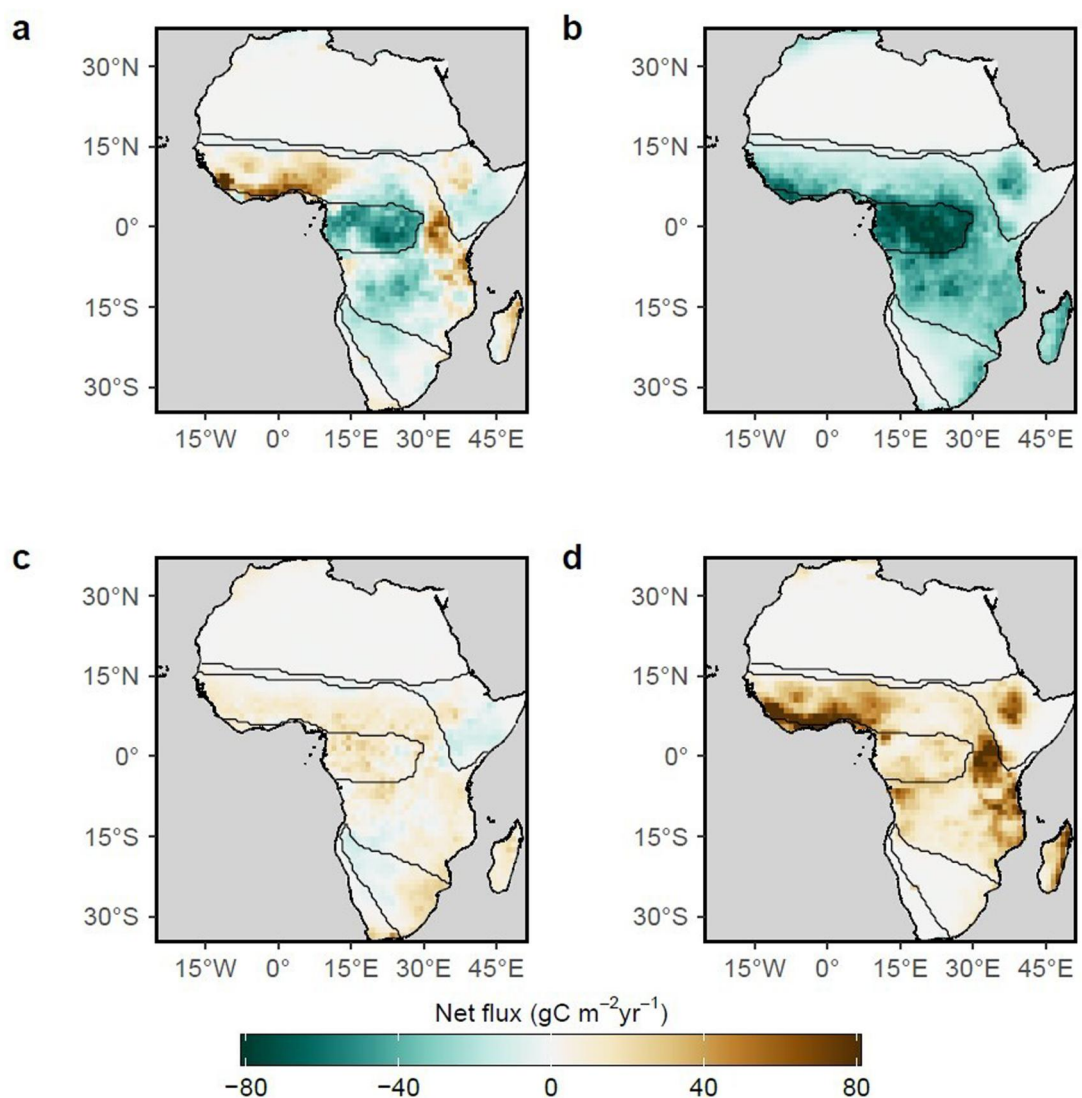


**Figure 3.** Spatial pattern of trends in annual mean NBP ( $\text{gC m}^{-2} \text{yr}^{-1}$ ) across Africa over 2000 to 2019 based on an ensemble of 17 Dynamic Global Vegetation Models from TRENDY v9. Large opposing fluxes result in a net sink of carbon (a), while (b) shows the attribution of  $\text{CO}_2$  fertilization and N deposits, (c) the attribution of climate change and variability and (d) the attribution of Land Use Change. Black isolines represent the boundaries of the ecoregions as depicted in Figure 1.

(Houghton & Nassikas, 2017):  $0.43 \pm 0.02 \text{ PgC yr}^{-1}$ . Climate-induced losses have decreased to almost zero (Table 4) likely due to the breaking of the decades-long drought in the Sahel, which compensated for increased aridity in East Africa over the same time period. Consequently, the biospheric sink capacity in Africa has increased to  $-0.09 \pm 0.24 \text{ PgC yr}^{-1}$  in the last decade. The LUC fluxes are spatially concentrated in the sub-humid savanna (a net source of  $0.04 \pm 0.17 \text{ PgC yr}^{-1}$ ), while most of the sink capacity is concentrated in the tropical forests ( $-0.08 \pm 0.06 \text{ PgC yr}^{-1}$ ). This estimated sink capacity is an order of magnitude lower than that estimated from models that do not include land use and land cover: Africa NEE (including fire disturbances) estimated by TRENDY model ensembles (Section 2.2.2) was  $-0.09 \pm 0.24 \text{ PgC yr}^{-1}$  in 2010–2019 compared with  $-2.21 \text{ PgC yr}^{-1}$  for aDGVM (Section 2.2.3).

We find large gross changes in the vegetation stocks but the net carbon stocks remain the same (Figure 4). Soil carbon pools are increasing: that is the DGVM models predict that the increase in  $\text{CO}_2$  uptake caused by  $\text{CO}_2$  fertilization continues to be larger than fluxes to the atmosphere due to increased microbial respiration rates, LUC and climate change.

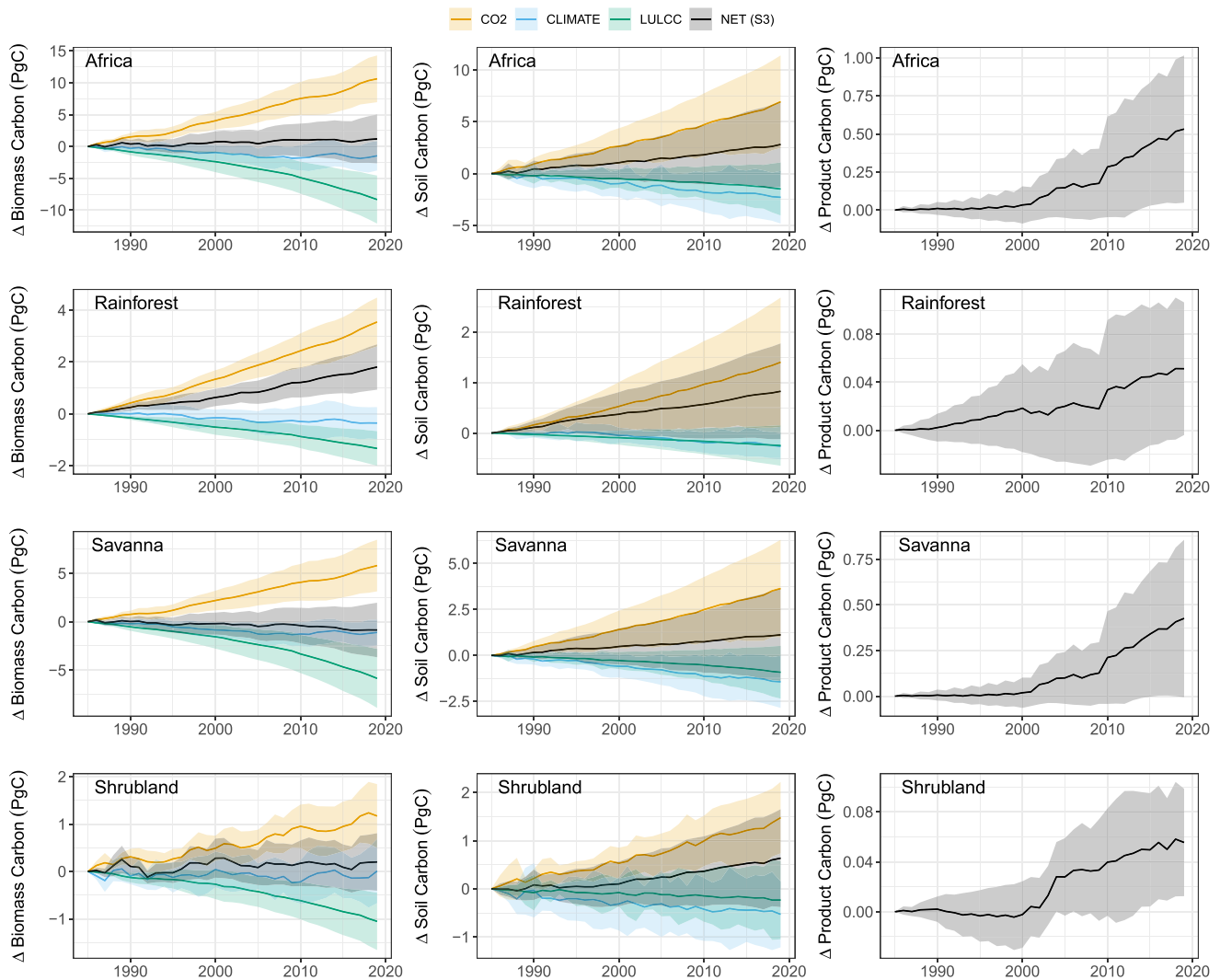


**Figure 4.** Change in carbon pools over the 1985 to 2019 period.

The TRENDY DGVM models vary in the processes simulated (see Table A1 in Friedlingstein et al. (2020a)). Most of them (11/17) simulate wildfires, and approximately half (8/17) include nitrogen fertilization. Fuelwood harvest was commonly simulated (11/17 times), but tillage, irrigation, mowing, and other land use activities are included by very few models, and none include peatland drainage. The TRENDY protocol used the HYDE 3.2 land use product (Klein Goldewijk, 2017), but DGVM models varied in how they interpreted and used these data (Friedlingstein et al., 2020a). HYDE 3.2, unlike some land use data sets, does not show a leveling off of cropland expansion in Africa over the RECCAP2 period (see Text S1 in Supporting Information S1): all of the models used here are simulating increased cropland of approximately  $50\text{--}100\text{ km}^2 \times 10^3\text{ yr}^{-1}$  whereas the HYDE 3.3 data set has cropland change of close to zero for most of the last decade (Figure 5). All of these factors might compound uncertainty in the TRENDY model estimates.

### 2.2.3. Ecosystem Models Without Land Use (aDVGM)

The aDVGM is an individual-based model that has been developed specifically to simulate grass-tree dynamics in African ecosystems (Scheiter & Higgins, 2009). It has been shown to simulate the distribution of grasslands, savannas, and forests in Africa, but detailed assessments of carbon fluxes have not been conducted (Martens et al., 2021; Scheiter & Higgins, 2009). The aDVGM only represents potential natural vegetation without any land

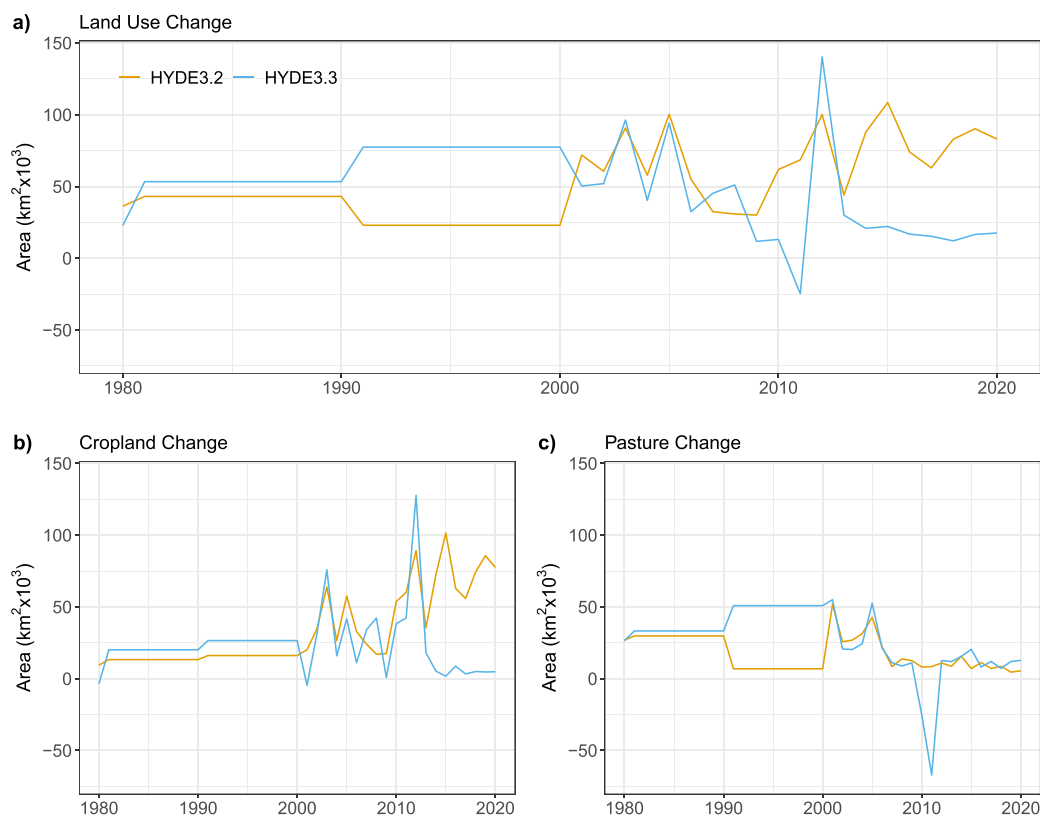


**Figure 5.** Change in area for (a) land use, (b) cropland and (c) pasture estimated from HYDE 3.2 (orange line) and HYDE 3.3 (blue line). HYDE 3.2 indicates increases in cropland area over the RECCAP2 period, but HYDE 3.3 indicates no change. See Supporting Information S1 for further information on uncertainty in land use change trends.

use driver (see Section 2.2.2 for results including land use). Here, aDGVM was forced with an ensemble of regionally-downscaled general circulation models over the 1985–2018 period.

In aDGVM simulated GPP, NPP, and NEE increased to 13.4, 7.4, and  $-3.0 \text{ PgC yr}^{-1}$  for the 2009–2018 period (Table 5). These GPP values are lower than estimates from satellite observation ( $22.4\text{--}24.7 \text{ PgC yr}^{-1}$  for different periods, Section 2.3.1, Table 3), and lower than values simulated by other DGVMs (GPP between 20.6 and  $40.9 \text{ PgC yr}^{-1}$ , NPP between 9.2 and  $20.5 \text{ PgC yr}^{-1}$  for an ensemble of nine models, Valentini et al., 2014); NPP of  $10.2 \text{ PgC yr}^{-1}$  for the period 1980–2009 in simulations for Africa (Pan et al., 2015); NPP of 10.2 and  $10.9 \text{ PgC yr}^{-1}$  in the presence and absence of fire (Sato & Ise, 2012). However, the NEE of the forest region simulated by aDGVM ( $-0.51 \text{ PgC yr}^{-1}$  for 1985–2008, increasing to  $-0.56 \text{ PgC yr}^{-1}$  for 2009–2018) is slightly higher than the estimate of  $-0.34 \text{ PgC yr}^{-1}$  (CI,  $-0.15$  to  $-0.43$ ) for observation data from sparse forest plots (Lewis et al., 2009). This supports results by Hubau et al. (2020) indicating that the forest carbon sink in intact African forests remained constant throughout the RECCAP2 period.

Both autotrophic and heterotrophic respiration increased in Africa according to aDGVM simulations (Table S5 in Supporting Information S1). Autotrophic respiration increased from  $1.03 \text{ PgC yr}^{-1}$  in the period 1985–2008 to  $1.19 \text{ PgC yr}^{-1}$  in the period 2009–2018, and heterotrophic respiration increased from 8.11 to  $8.82 \text{ PgC yr}^{-1}$  over the same periods. The highest respiration rates were simulated in the Sub-humid savanna region (0.65 and  $4.72 \text{ PgC yr}^{-1}$  for autotrophic and heterotrophic respiration in 2009–2018). Valentini et al. (2014) reported a multi-model mean heterotrophic respiration  $11.8 \text{ PgC yr}^{-1}$ , which is higher than the aDGVM simulations.

In aDGVM simulations, carbon stored aboveground in Africa was 59.5 PgC in the period 2009–2018 (Table 5). This is lower than values by other models; 66.7 to 181.4 PgC for an ensemble of nine models (Valentini et al., 2014); 75.3 to 87.5 PgC with SEIB-DGVM (Sato & Ise, 2012); but falls within the range of estimates (48.3–

**Table 5***Carbon Stocks and Fluxes Simulated by aDGVM*

Carbon stocks	Region	AboveGround (PgC)		Belowground (PgC)		Soil (PgC)		Total (PgC)		Trend (Pg Cyr <sup>-1</sup> )	
		1985–2008	2009–2018	1985–2008	2009–2018	1985–2008	2009–2018	1985–2008	2009–2018	1985–2008	2009–2018
Total carbon	NH Desert	0.95	1.05	0.59	0.67	4.22	4.33	5.76	6.06	0.02	0.04
	Forest	18.85	19.66	3.68	3.92	12.75	13.29	35.29	36.86	0.08	0.10
	Desert/Shrubland	0.26	0.29	0.13	0.15	1.00	1.03	1.39	1.47	0.002	0.004
	Sub-humid savanna	28.20	30.97	11.68	12.91	39.32	40.98	79.20	84.87	0.29	0.40
	Semi-arid savanna	6.69	7.58	3.91	4.42	16.37	17.15	26.98	29.14	0.10	0.13
	Africa	54.95	59.54	20.01	22.08	73.66	76.77	148.63	158.40	0.49	0.67
Carbon fluxes	Region	Total (Pg Cyr <sup>-1</sup> )		Trend (PgC yr <sup>-1</sup> )							
		1985–2008	2009–2018	1985–2008	2009–2018						
NPP	NH Desert	0.23	0.28	0.00	0.01						
	Forest	1.15	1.24	0.01	0.01						
	Desert/Shrubland	0.06	0.06	0.00	–0.00						
	Sub-humid savanna	3.82	4.14	0.02	0.04						
	Semi-arid savanna	1.50	1.68	0.01	0.01						
	Africa	6.75	7.40	0.04	0.06						
GPP	NH Desert	0.41	0.50	0.01	0.02						
	Forest	2.23	2.40	0.01	0.01						
	Desert/Shrubland	0.10	0.11	0.00	–0.00						
	Sub-humid savanna	6.86	7.45	0.03	0.07						
	Semi-arid savanna	2.63	2.94	0.02	0.02						
	Africa	12.22	13.41	0.07	0.11						
NEE	NH Desert	–0.06	–0.09	–0.00	–0.01						
	Forest	–0.51	–0.56	–0.00	–0.00						
	Desert/Shrubland	0.00	–0.01	0.00	0.00						
	Sub-humid savanna	–1.62	–1.78	–0.01	–0.03						
	Semi-arid savanna	–0.52	–0.60	–0.01	–0.01						
	Africa	–2.72	–3.04	–0.02	–0.04						

*Note.* Variables are averaged for whole Africa and ecoregions for the periods 1985–2008 and 2009–2018 and stocks include Aboveground, Belowground and Soil. Trends were derived by linear regression models using time series of monthly means of the respective variable. Detailed results in Supporting Information S1. Some values are zero due to rounding.

64.5 PgC) by remote sensing AGB products (Avitabile et al., 2016; Baccini et al., 2012; Y. Y. Liu et al., 2015; Saatchi et al., 2011). Those remote sensing products do however represent slightly different periods within the RECCAP2 time period.

Aboveground carbon increased by 4.6 PgC between 2009 and 2018, with the highest increases in Sub-humid savannas. Belowground biomass increased by 2 PgC, and SOC increased by 3.1 PgC (Table 5), the overall rate of increase estimated without land use activities is 0.67 PgC yr<sup>-1</sup> which is higher than for the 1985–2008 period.

### 2.3. Fluxes of Special Importance Within the African GHG Budget

#### 2.3.1. Fires

Recent decades have seen reductions in the area burned per year in Africa from  $\sim 3.1 \times 10^6$  km<sup>2</sup> to  $\sim 2.6 \times 10^6$  km<sup>2</sup> (Andela et al., 2017; Zubkova et al., 2019) and consequently also a decline in total fire emissions (Figure 6) (Van

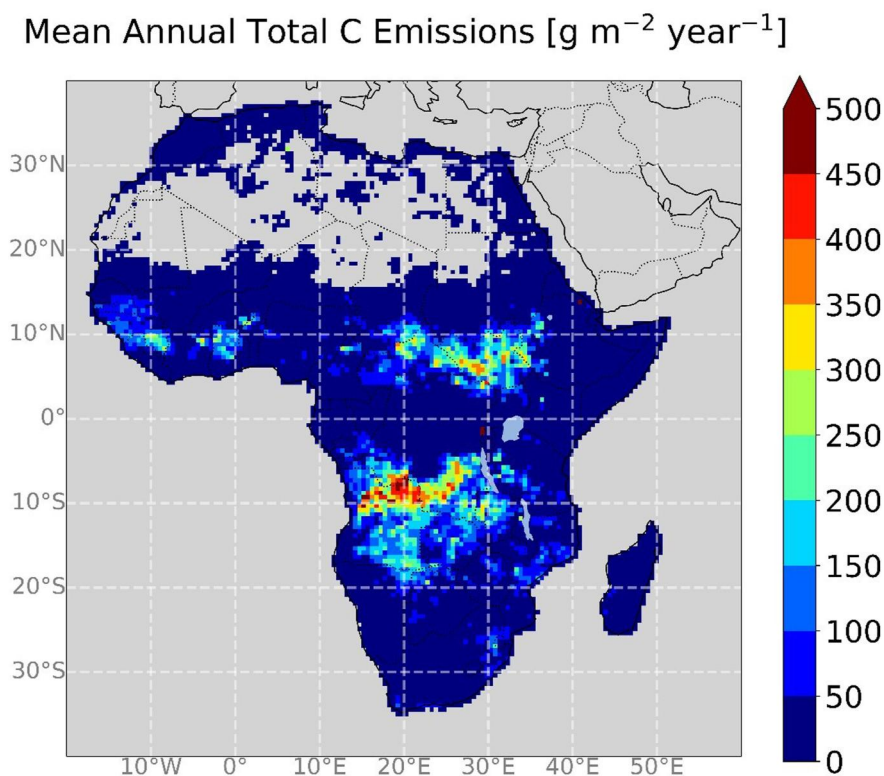


**Figure 6.** Spatial patterns of biomass burning emissions in Africa calculated from the FREMV2.1.

Der Werf et al., 2017). Approximately 30% of this decline is attributed to land transformation and expansion of agricultural land (Zubkova et al., 2019); therefore, this does not necessarily imply increased C-sink potential. However the remaining ~70% appears to be a result of higher effective rainfall and soil moisture, particularly in North Africa, producing less flammable vegetation (Zubkova et al., 2019).

Emissions estimates from wildfire come from bottom up (based on burned area) and top-down (based on fire radiative power) methods (see Text S3 in Supporting Information S1). Several new data products have become available since the RECCAP1 period. Current bottom up burned area products omit small fires and analyses with higher resolution SENTINEL-2 data nearly double the estimated burned area (Roteta et al., 2019), possibly also doubling the estimated GFED fire emissions (Ramo et al., 2021). Here we present a new Africa-specific top-down fire emissions product (Nguyen & Wooster, 2020) and contrast it with estimates from other sources (Table 6).

Existing estimates of total carbon emissions from wildfires in Africa range from 954 to 1,595  $\text{Tg C yr}^{-1}$ , with  $\text{CH}_4$  ranging from 4.9 to 9.1  $\text{Tg CH}_4 \text{ yr}^{-1}$  and  $\text{N}_2\text{O}$  from 0.8 to 0.4  $\text{Tg N}_2\text{O yr}^{-1}$  (Table 6). Of these emissions, ~85% come from sub-humid savannas which, due to their high productivity and long dry seasons, produce frequent fires that consume high amounts of biomass. Both top-down (calculated via energy released) and bottom-up approaches (calculated via burned area) show a clear decline over the last two decades (Table 6; Figure 7) in the order of ~10  $\text{Tg C yr}^{-1}$ . In contrast, total carbon emissions from wood fuel burning have increased steadily from  $184 \pm 24.6 \text{ Tg C yr}^{-1}$  for RECCAP1 to approximately  $242 \pm 36.1 \text{ Tg C yr}^{-1}$  for the RECCAP2 period (see Table S6 in Supporting Information S1 for more details). This represents an increase of approximately 5.3  $\text{Tg C yr}^{-1}$ . Total fire emissions (wildfire and fuel wood burning) have therefore decreased slightly from  $1,225 \pm 99$  to  $1,197 \pm 85 \text{ Tg C yr}^{-1}$ . Of these fire emissions, approximately 134  $\text{Tg C}$  (or ~12%) are considered a net source (Bailis et al., 2015; Scholes et al., 2011; van der Werf et al., 2017).

### 2.3.2. Large Mammals

Herbivore  $\text{CH}_4$  emissions represent a small but increasing component of the African methane cycle, which is highly uncertain (Valentini et al., 2014). African livestock production systems differ from global averages in



**Table 6**

*Comparing the Change in Mean Annual Emissions (Tg yr<sup>-1</sup>) for Different Chemical Species for Wildfires (Including Deforestation and Cropland Fires) and Fuelwood Burning Over the RECCAP1 and RECCAP2 Periods*

Type	Source	Region	RECCAP1 <sup>a</sup>	RECCAP2 2010-2019	Trend: Change/yr
Wildfire	Valentini	Africa	1031 (±87)		
	FREMV2.1	Africa	999 (±79)	953 (±113)	-10.9
		Northern Hemisphere		377	
		Southern Hemisphere		576	
		Forest		26	
		NH Desert		4	
		SH Desert		3	
		Sub-humid savanna		810	
		Semi-arid savanna		124	
FuelWood	Various (see SI)	Africa	184	241	5.3
Total C	wildfire + fuelwood		1,215	1,194	-9
Total CO <sub>2</sub>	FREM (range)			3,250 (2,225–5,475)	
Total CH <sub>4</sub>	FREM (range)			6.8 (4.9–9.1)	
Total CO	FREM (range)			146 (142–224)	
Total N <sub>2</sub> O	FREM (range)			0.09 (0.09/0.42)	

*Note.* Fuelwood burning was calculated from published sources (Amos, 1999; Bailis et al., 2015; Boden et al., 2013; Broadhead et al., 2001; FAO, 2010) integrated with the IEA World Energy Balances statistics (IEA, 2022). Estimates come from FREMV2.1, a top-down regional product derived specifically for Africa (slightly modified from Nguyen & Wooster, 2020). Estimates for CO, CH<sub>4</sub>, and N<sub>2</sub>O emissions for RECCAP2 period are also provided, showing the FREMV2.1 estimate and the range of other estimates for that time period. See Supporting Information S1 for more details of wildfire emissions data sources and the wood fuel burning estimates. <sup>a</sup>Valentini et al. (2014) reported from 1997 to 2011, and FREMV2.1 was available from 2004 to 2009.

terms of diet, average body weights, herd structure, and body condition (Goopy et al., 2021; Ndung'u et al., 2022). The IPCC 2019 methodology estimates emission factors for free-ranging cattle in low productivity systems of Africa to be 48 kgCH<sub>4</sub>/head yr<sup>-1</sup> (Table 10.11 in IPCC, 2019), but recent empirical papers from Africa report emissions factors closer to the IPCC 2006 estimate of 31 kgCH<sub>4</sub>/head yr<sup>-1</sup> (Table S9 in Supporting Information S1).

Livestock represents 98% of the herbivore biomass in Africa (Hempson et al., 2017), and emissions from manure are small (<3%, Herrero et al., 2008); therefore, we focused here on enteric fermentation from livestock, whose numbers have increased by 30% in Africa in the last decade (Gilbert et al., 2018). The 11 African countries that regularly report livestock emissions to the UNFCCC showed livestock methane emissions increasing by ~5% between the RECCAP1 and RECCAP2 periods, but the IPCC Tier 1 approach estimates increases closer to 30% for the same 11 countries. We produced a new African livestock emission factor (Africa\_EF) calculated using the mean of a range of empirical data sources from African livestock production systems (see Table S9 in Supporting Information S1) of 35.6 kgCH<sub>4</sub>/head yr<sup>-1</sup>. When using Africa\_EF instead of the IPCC value of 48 kgCH<sub>4</sub>/head yr<sup>-1</sup> the overall methane emissions are reduced, but the increasing trend remains the same.

Models using metabolically based methane emissions model and different production systems (Herrero et al., 2008; Wolf et al., 2017) are less than half the IPCC 2019 Tier 1 approach (Table 7) and only show a 13% increase between the two periods caused both by increasing livestock numbers and a switch to more mixed production systems. The current best estimate of CH<sub>4</sub> emissions from enteric fermentation of livestock in Africa for the RECCAP2 period is 17.6 (range 9.2–21.7) TgCH<sub>4</sub> yr<sup>-1</sup> which represents an annual increase of 2.9% (395 GgCH<sub>4</sub> yr<sup>-1</sup>) from RECCAP1.

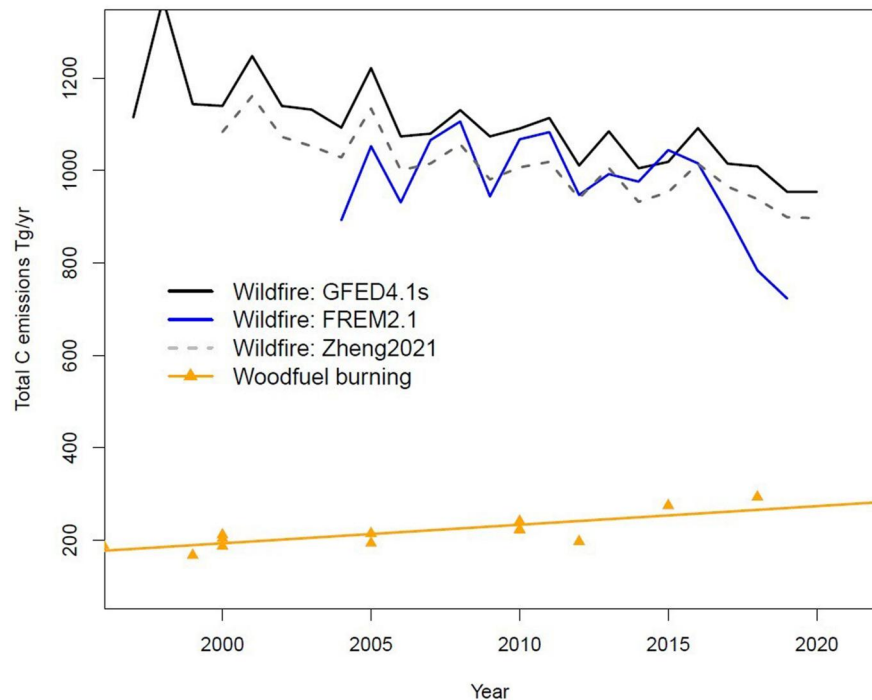


**Figure 7.** Total carbon emissions from wildfires are decreasing while fuel wood emissions are increasing. Wildfire estimates are provided for a “bottom up” data product (GFED4.1s) (Randerson et al., 2017; Van Der Werf et al., 2017), a global “top-down” data product derived from an atmospheric inversion applied to MOPITT satellite CO data (Zheng et al., 2021), and a regional “top-down” data set for Africa derived from correlations between FRP and TPM and CO (FREMv2.1 slightly modified from Nguyen and Wooster (2020)). See Table 6 for the range of current estimates for all greenhouse gases.

**Table 7**

Estimates of Annual Enteric Methane Emissions ( $\text{TgCH}_4 \text{ yr}^{-1}$ ) for Africa Calculated Using the IPCC Tier 1 Methodology (IPCC, 2019) and the Tier 1 Methodology With Africa-Specific Emissions Factors (IPCC2019\_AfricaEF), Contrasted With Estimates From Published Sources, and From National UNFCCC Reporting

	2000–2009	2010–2019	Trend: $\text{GgCH}_4 \text{ yr}^{-1}$
UNFCCC (11 reporting countries)			
UNFCCC	5.1 ( $\pm 0.3$ )	5.3 ( $\pm 0.1$ )	27
IPCC2019	5.2	6.8	161
IPCC2019_AfricaEF	4.1	5.4	131
Africa			
Herrero et al. (2008)	8.1	9.2	109
Wolf et al. (2017)	12.7 $\pm$ 1.9		
IPCC2019	16.8	21.7	482
IPCC2019_AfricaEF	13.7	17.6	395

*Note.* IPCC2019 uses emission factors from Table 10.11 which has a cattle emission factor of 48 for low-productivity systems. This is higher than all published emission factors for free-ranging cattle in Africa (See Table S9 in Supporting Information S1), so the IPCC2019\_AfricaEF replaces this with the mean reported value of  $35.6 \text{ kgCH}_4/\text{head yr}^{-1}$ . Only 11 countries have UNFCCC data for both RECCAP periods so data are reported for these 11 countries, and for Africa as a whole.

### 2.3.3. Termites

Termites are an important source of methane due to the methanogenic degradation of lignocellulose in termite hindguts (Brune, 2014). The African continent hosts 39% of the total 2,600 species that have been described worldwide (Ahmed et al., 2011), contributing substantially to global termite  $\text{CH}_4$  emissions. Here, we provide new estimates of termite  $\text{CH}_4$  emissions across the African continent (Figure 8, Table 8) based on a new global termite biomass product predicted from 500 field transect measurements using a machine learning approach and the global mean and median of termite  $\text{CH}_4$  production rate from existing literature (mean =  $3.74 \mu\text{gCH}_4 \text{ g}^{-1}[\text{termite}] \text{ h}^{-1}$ , median =  $2.88 \mu\text{gCH}_4 \text{ g}^{-1}[\text{termite}] \text{ h}^{-1}$ ,  $n = 251$ ) (Zhou et al., 2023). Overall, termites across the African continent are predicted to emit  $1.40 \text{ TgCH}_4 \text{ yr}^{-1}$  (the 95% confidence intervals range:  $1.31\text{--}1.49 \text{ TgCH}_4 \text{ yr}^{-1}$ ) based on the mean termite  $\text{CH}_4$  production rate, with the largest emission from sub-humid savannas ( $0.63 \text{ TgCH}_4 \text{ yr}^{-1}$ ) followed by semi-arid savanna ( $0.37 \text{ TgCH}_4 \text{ yr}^{-1}$ ) and forests ( $0.19 \text{ TgCH}_4 \text{ yr}^{-1}$ ) (also see Table 8 for the median estimate of termite  $\text{CH}_4$  production rate).

This new estimate is substantially lower than the estimate of  $2.09 \text{ TgCH}_4 \text{ yr}^{-1}$  from the global methane budget (Saunois et al., 2020) (Table 8) and other reported values ( $2.5\text{--}6.9 \text{ TgCH}_4 \text{ yr}^{-1}$ ) from Valentini et al. (2014) for the African continent. Two prominent reasons for these inconsistencies are the lack of accurate data on termite biomass for upscaling, and the scarcity of empirical data on termite  $\text{CH}_4$  emission rates. Termite biomass is generally estimated by its dependence on GPP of ecosystems based on simple regression models (Kirschke et al., 2013; Saunois et al., 2020). Here, our global

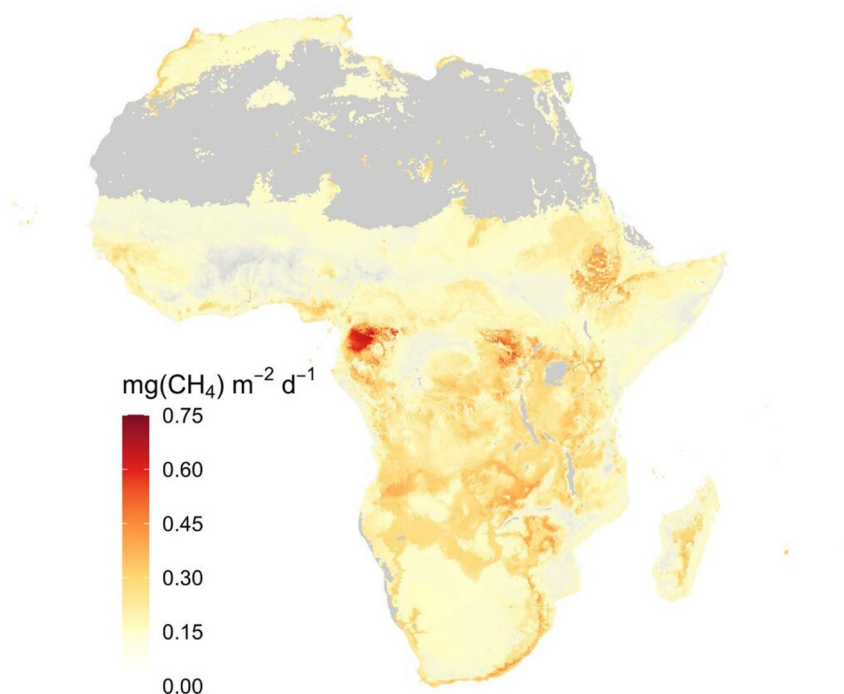


**Figure 8.** Methane emission rates ( $\text{mgCH}_4 \text{ m}^{-2} \text{ d}^{-1}$ ) from termites are estimated across the African continent.

termite biomass estimate is based on available field measurements and predicted by a set of variables, including rainfall, soil pH, NPP, minimum/maximum temperature, SOC, and topography. Additionally, only a few studies measured  $\text{CH}_4$  emission rates at the individual species or mound scale across the African continent (Table S10 in Supporting Information S1) with  $\text{CH}_4$  emission rates varying significantly between species ( $0.68\text{--}17.4 \mu\text{g CH}_4 \text{ g}^{-1} \text{ hr}^{-1}$ ), between mounds ( $81\text{--}5,478 \text{ ng CH}_4 \text{ s}^{-1} \text{ mound}^{-1}$ ) (Brauman et al., 2001; Macdonald et al., 1999; Rouland et al., 1993) and between seasons (Räsänen et al., 2023). However, more empirical measurements are still needed to improve the accuracy of termite biomass as well as termite methane emission rates across different ecosystems and regions.

**Table 8**  
*Predicted Termite Methane Emissions Across African Ecoregions*

Ecoregion	Termite methane emissions ( $\text{TgCH}_4 \text{ yr}^{-1}$ )		
	Saunois et al. (2020)	New estimate based on mean termite $\text{CH}_4$ production rate	New estimate based on median termite $\text{CH}_4$ production rate
North Africa desert	0.067	0.134 (0.123–0.145)	0.103 (0.094–0.111)
Desert/shrubland	0.021	0.039 (0.036–0.042)	0.030 (0.028–0.032)
Semi-arid savanna	0.354	0.367 (0.342–0.392)	0.282 (0.263–0.301)
Sub-humid savanna	1.220	0.629 (0.589–0.670)	0.484 (0.452–0.516)
Forest	0.350	0.185 (0.175–0.195)	0.142 (0.134–0.150)
Africa (in total)	2.094	1.397 (1.305–1.489)	1.076 (1.004–1.247)

*Note.* Values in parentheses represent the 95% confidence intervals.

## 2.4. Component Fluxes of NEE From Geological, Aquatic, and Coastal Systems

### 2.4.1. Geological Carbon Emissions

Africa's geogenic CO<sub>2</sub> emissions are mostly due to volcanic and geothermal activity in the East African Rift (EAR), which is globally the largest active continental rift spanning a cumulative length of approximately 3,000 km (Lee et al., 2016). Extrapolation from first-order CO<sub>2</sub> flux measurements of tectonic degassing in the Magadi-Natron basin amounts to a flux of  $71 \pm 33$  TgCO<sub>2</sub> yr<sup>-1</sup> in the EAR (Lee et al., 2016). However, estimates based on extrapolation from surveys in the Main Ethiopian Rift (0.52–4.36 TgCO<sub>2</sub> yr<sup>-1</sup>) give a flux range of 3.9–32.7 TgCO<sub>2</sub> yr<sup>-1</sup> (Hunt et al., 2017).

Geological emission sources of CH<sub>4</sub> were calculated for each ecoregion and Africa as a whole using data from Etiope et al. (2019) (Table 9, Table S11 in Supporting Information S1). These include emissions from onshore seeps (gas-oil seeps and mud volcanoes), diffuse exhalation of CH<sub>4</sub> associated with petroleum fields (micro-seepage) and geothermal manifestations mainly from volcanoes and geothermal sites, but excluding submarine seeps (see Ciais et al., 2022). The North African desert ecoregion contributes 46% of the estimated total African geological CH<sub>4</sub> emissions of 1.01 TgCH<sub>4</sub> yr<sup>-1</sup> (see Figure S3 in Supporting Information S1 for the spatial distribution). Semi-arid and Sub-humid savanna ecoregions contribute 30% and 20%, respectively, while the forest ecoregion only contributes 5% of the estimated geological CH<sub>4</sub> emissions across Africa.

### 2.4.2. Weathering Uptake of Atmospheric CO<sub>2</sub>

We extracted estimates of weathering CO<sub>2</sub> uptake and the weathering dissolved inorganic carbon (DIC) release from gridded products provided by Lacroix et al. (2020) for the African ecoregions (Table 9, Table S12 in Supporting Information S1). The method quantifies weathering and depends on surface runoff and temperature, lithology types and soil shielding, and is based on a modified version of the weathering model of Hartmann et al. (2009). Weathering on the continent induces a flux of  $-12.2$  Tg C yr<sup>-1</sup> of CO<sub>2</sub>, accounting for around 7% of the global weathering consumption. The sink estimate for the continent is comparable with the previous estimate of  $-11.7$  Tg C yr<sup>-1</sup> of Ludwig et al. (1998). The carbon uptake from the atmosphere and carbon originating from the rock material add up to a total of  $-15.2$  Tg C yr<sup>-1</sup> DIC exported to freshwaters and the ocean. Lacroix et al. (2020) reported that there was a general underestimation of catchment DIC exports for African catchments, for example, a 20% underestimation compared to measurements for the Congo basin.

In Africa, the lowest consumption rates ( $0-0.1$  tC km<sup>-2</sup> yr<sup>-1</sup>) were recorded over eastern and southern Africa, while larger amounts ( $0.5-5$  tC km<sup>-2</sup> yr<sup>-1</sup>) of CO<sub>2</sub> were consumed in central Africa and parts of East Africa. The Semi-arid savanna ecoregion, which consists, to a large degree, of metamorphics, unconsolidated and silicoclastic sediment lithological classes, accounts for the highest weathering rates per area and the largest part of the continent's weathering drawdown and DIC release (Table 9, Table S12 in Supporting Information S1), owing to rather high runoff rates ranging from 50 to 250 mm yr<sup>-1</sup>. Weathering rates in warm and runoff-abundant tropical forest areas are strongly reduced due to shielding by old and highly weathered soils (Hartmann et al., 2014), whereas weathering in the dry semi-arid savanna and desert is limited by precipitation and runoff, which is predominantly less than 25 mm yr<sup>-1</sup>.

### 2.4.3. Inland Water Emissions

Emissions of CO<sub>2</sub>, CH<sub>4</sub>, and N<sub>2</sub>O from rivers and lakes were taken from the regional estimates by Borges et al. (2015), Borges, Deirmendjian, Bouillon, Okello, et al. (2022) which provide average annual emissions of 990–1,360 TgCO<sub>2</sub> yr<sup>-1</sup>, 3.9–5.2 TgCH<sub>4</sub> yr<sup>-1</sup> and 14.8–19.8 GgN<sub>2</sub>O yr<sup>-1</sup> from African rivers, and annual emissions of 12.1 TgCO<sub>2</sub> yr<sup>-1</sup> and 2.2 TgCH<sub>4</sub> yr<sup>-1</sup> from African lakes, but explicitly excluded reservoirs (Table 9). Moreover, they suggest that African lakes can be a minor sink of 0.2 GgN<sub>2</sub>O yr<sup>-1</sup> (Borges, Deirmendjian, Bouillon, Okello, et al., 2022). For reservoir emissions, we used numbers provided in the synthesis of regionalized inland water emission estimates by Lauerwald et al. (2023a) for the RECCAP2 initiative. These estimated emission amount to 16 (7/26) TgCO<sub>2</sub> yr<sup>-1</sup>, 2.1 (1.2/3.1) TgCH<sub>4</sub> yr<sup>-1</sup> and 6.6 (2.7/8.6) GgN<sub>2</sub>O yr<sup>-1</sup> (Lauerwald et al., 2023a). Summing up these estimates, we get to total emission fluxes of 1.11 (0.87/1.35) PgCO<sub>2</sub> yr<sup>-1</sup>, 9 (7/11) TgCH<sub>4</sub> yr<sup>-1</sup>, and 0.027 TgN<sub>2</sub>O yr<sup>-1</sup> from African inland waters (Table 9). It is noteworthy that rivers contribute 98% of inland water CO<sub>2</sub> emissions, but only about half of inland water CH<sub>4</sub> emissions. To

**Table 9**  
*Geological, Inland Water and Coastal CO<sub>2</sub>, CH<sub>4</sub>, N<sub>2</sub>O, and Net GHG Emissions and Sinks*

Geological sources <sup>a</sup>	CO <sub>2</sub> (Tg yr <sup>-1</sup> ) 18.3 (3.9/32.7)	CH <sub>4</sub> (Tg yr <sup>-1</sup> ) 1 (1/1)	N <sub>2</sub> O (Gg yr <sup>-1</sup> )	CO <sub>2</sub> eq (GWPI00) (Tg yr <sup>-1</sup> ) 45.7 (31.3/60.1)	C (Tg yr <sup>-1</sup> ) 5.8 (1.8/9.7)
Atmospheric fluxes					
Lakes <sup>b</sup>	12.1 (12.1/12.1)	2.2 (2.2/2.2)	-0.2 (-0.2/-0.2)	71.4 (71.4/71.4)	5 (5/5)
Reservoirs <sup>c</sup>	16.2 (6.8/26.1)	2.1 (1.2/3.1)	6.6 (2.7/8.6)	74.7 (39.9/111)	5.7 (1.9/9.4)
Rivers <sup>b</sup>	1,175 (990/1,360)	4.6 (3.9/5.2)	17.3 (14.8/19.8)	1,302.6 (1,099.3/1,505.8)	322.4 (271.7/373.1)
Estuary Emissions (Tidal systems and lagoons) <sup>d</sup>	21.6 (12.7/32.4)	0 (0/0.1)	2.8 (2.5/3.2)	23.3 (13.4/37.3)	5.9 (2.5/9.6)
Coastal Wetland Emissions (Mangroves, Salt marshes, Seagrasses) <sup>d</sup>	-118.8 (-149.1/-82)	0.1 (0.1/0.3)	0.1 (0.1/0.3)	-116 (-147.1/-73.4)	-32.4 (-45.8/-22.5)
Net aquatic atmospheric fluxes	1,106.2 (872.5/1,348.6)	9 (7.4/10.9)	26.6 (19.8/31.8)	1,356.1 (1,076.9/1,652.2)	306.6 (235.2/374.7)
Carbon stock change					
OC burial— <i>inland</i> <sup>e</sup>	-131.9 (-24.1/-212.6)	0 (0/0)	0 (0/0)	-131.9 (-24.1/-212.6)	-36 (-6.6/-58)
OC burial— <i>coastal</i> <sup>d</sup>	-20.9 (-20.9/-20.9)	0 (0/0)	0 (0/0)	-20.9 (-20.9/-20.9)	-5.7 (-5.7/-5.7)
Net aquatic carbon stock change	-152.8 (-45/-233.5)	0 (0/0)	0 (0/0)	-152.8 (-45/-233.5)	-41.7 (-12.3/-63.7)
Lateral fluxes					
DIC <sup>f</sup>	-55.7 (-55.7/-55.7)	0 (0/0)	0 (0/0)	-55.7 (-55.7/-55.7)	-15.2 (-15.2/-15.2)
DOC <sup>g</sup>	-71.4 (-71.4/-71.4)	0 (0/0)	0 (0/0)	-71.4 (-71.4/-71.4)	-19.5 (-19.5/-19.5)
POC <sup>g</sup>	-64.6 (-64.6/-64.6)	0 (0/0)	0 (0/0)	-64.6 (-64.6/-64.6)	-17.6 (-17.6/-17.6)
Coastal Margin C inputs <sup>d</sup>	-458.3 (-187/-729.7)	0 (0/0)	0 (0/0)	-458.3 (-187/-729.7)	-125 (-51/-199)
Net aquatic lateral fluxes	-650 (-378.6/-921.3)	0 (0/0)	0 (0/0)	-650 (-378.6/-921.3)	-177.3 (-103.3/-251.3)

<sup>a</sup>Hunt et al. (2017), Etiope et al. (2018), Section 2.5.1. <sup>b</sup>Borges et al. (2015), Borges, Deirmendjian, Bouillon, Okello, et al. (2022). <sup>c</sup>Lauerwald et al. (2023b). <sup>d</sup>RECCAP2 database (<https://www.bgc-jena.mpg.de/geodb/projects/Data.php>). <sup>e</sup>Mendonça et al. (2017). <sup>f</sup>Lacroix et al. (2020), Section 2.5.2. <sup>g</sup>Zscheischler et al. (2017).



**Table 10**  
*Crop and Wood Trade Fluxes ( $\pm$ Inter-Annual Variability) in  $\text{TgCO}_2 \text{ yr}^{-1}$  and  $\text{TgCyr}^{-1}$* 

Period	1961–1984		1985–2009		2010–2019	
	$\text{TgCO}_2 \text{ yr}^{-1}$	$\text{TgCyr}^{-1}$	$\text{TgCO}_2 \text{ yr}^{-1}$	$\text{TgCyr}^{-1}$	$\text{TgCO}_2 \text{ yr}^{-1}$	$\text{TgCyr}^{-1}$
Crop export	$-13.6 \pm 2.3$	$-3.7 \pm 0.6$	$-14.9 \pm 4.0$	$-4.0 \pm 1.1$	$-29.1 \pm 10.8$	$-7.9 \pm 2.9$
Crop import	$22.6 \pm 13.2$	$6.1 \pm 3.6$	$73.6 \pm 23.9$	$19.9 \pm 6.5$	$137.2 \pm 45.3$	$37.2 \pm 12.2$
<b>Crop Net flux</b>	<b><math>9.0 \pm 13.4</math></b>	<b><math>2.4 \pm 3.6</math></b>	<b><math>58.6 \pm 24.2</math></b>	<b><math>15.8 \pm 6.5</math></b>	<b><math>108.7 \pm 46.6</math></b>	<b><math>33.2 \pm 12.6</math></b>
Wood export	$-3.9 \pm 0.7$	$-1.1 \pm 0.2$	$-7.7 \pm 3.3$	$-2.1 \pm 0.9$	$-9.9 \pm 3.3$	$-2.7 \pm 0.9$
Wood import	$1.6 \pm 0.6$	$0.4 \pm 0.2$	$4.2 \pm 2.3$	$1.1 \pm 0.6$	$9.9 \pm 3.6$	$2.7 \pm 1.0$
<b>Wood Net flux</b>	<b><math>-2.3 \pm 1.0</math></b>	<b><math>-0.6 \pm 0.3</math></b>	<b><math>-3.4 \pm 4.0</math></b>	<b><math>-0.9 \pm 1.1</math></b>	<b><math>0.05 \pm 4.9</math></b>	<b><math>0.3 \pm 1.3</math></b>

Note. Positive values represent imports (source) and negative values represent exports (sink).

quantify DOC and POC, we summarized data from Zscheischler et al. (2017), and freshwater burial was quantified from Mendonça et al. (2017).

#### 2.4.4. Fluxes From Estuaries and Coastal Wetlands

Emissions of  $\text{CO}_2$ ,  $\text{CH}_4$ , and  $\text{N}_2\text{O}$  from various coastal ecosystems in Africa were estimated using available empirical data scaled to the total surface area of each of the coastal ecosystems (Table 9). These systems include tidal systems and deltas, lagoons, mangroves, salt marshes and seagrasses. Organic carbon burial and coastal margin (non-riverine) C inputs were also estimated. However, although the coastal margin C sink is likely to be substantial, methodology is not yet resolved enough to calculate at the regional scale. To deal with this highly uncertain estimate, we therefore included the (rough) estimate in Table 9 for reporting purposes, but for the final budgets we set the mean value to zero and the 95th quantile as our best estimate. Hereby, the coastal margin sink is not represented in the final budgets, but the uncertainty has been accounted for.

### 2.5. Trade Fluxes

#### 2.5.1. Carbon in Crop and Wood Trade

The transfer of physical and embodied carbon to and from Africa represents a relatively small percentage when compared to the rest of the world (Peters et al., 2012). We consider the physical flows of carbon via trade in biomass that includes crops and harvested wood products for three different periods, including 1961–1984, 1985–2008, and 2009–2019, based on inventory data from the Food and Agricultural Organization of the United Nations database (FAOSTAT, 2021).  $F_{\text{trade}}$  is considered a carbon flux source by the region if it imports more than it exports or a carbon flux sink if it does not.

Africa was a net importer of crops during all three periods (Table 10). Carbon imports through crops increased more than six-fold in the 1985 to 2008 period from the 1961 to 1984 period and almost doubled from the 1985–2009 to 2010–2019 periods. From 1961 to 2009, Africa was a small net exporter of carbon through wood. During

**Table 11**  
*Anthropogenic Greenhouse Gas Emissions for the 1990–2009 (R1) and 2010–2019 (R2) Periods*

Period	Anthropogenic emissions ( $\text{PgCO}_2$ -equivalent $\text{yr}^{-1}$ )					
	Fossil fuels (including industrial processes)	Waste	Agriculture	LUC	Total incl LUC	Bunkers ( $\text{Tg CO}_2$ -eq $\text{yr}^{-1}$ )
$\text{CO}_2$	R1	$0.83 \pm 0.11$		$0.98 \pm 0.02$	$1.81 \pm 0.13$	$37.1 \pm 3.83$
	R2	$1.28 \pm 0.06$		$1.20 \pm 0.07$	$2.48 \pm 0.12$	$41.6 \pm 1.69$
$\text{CH}_4$	R1	$0.35 \pm 0.04$	$0.13 \pm 0.02$	$0.44 \pm 0.05$	$0.99 \pm 0.08$	$0.04 \pm 0.01$
	R2	$0.38 \pm 0.02$	$0.16 \pm 0.01$	$0.61 \pm 0.03$	$1.21 \pm 0.04$	$0.02 \pm 0.01$
$\text{N}_2\text{O}$	R1	$0.06 \pm 0.02$	$0.01 \pm 0.00$	$0.28 \pm 0.03$	$0.36 \pm 0.05$	$0.24 \pm 0.03$
	R2	$0.08 \pm 0.00$	$0.02 \pm 0.00$	$0.36 \pm 0.01$	$0.46 \pm 0.01$	$0.28 \pm 0.02$
Total	R1	$1.23 \pm 0.12$	$0.15 \pm 0.02$	$0.73 \pm 0.06$	$1.09 \pm 0.03$	$37.4 \pm 3.83$
	R2	$1.74 \pm 0.06$	$0.19 \pm 0.01$	$0.97 \pm 0.03$	$1.31 \pm 0.07$	$41.9 \pm 1.69$

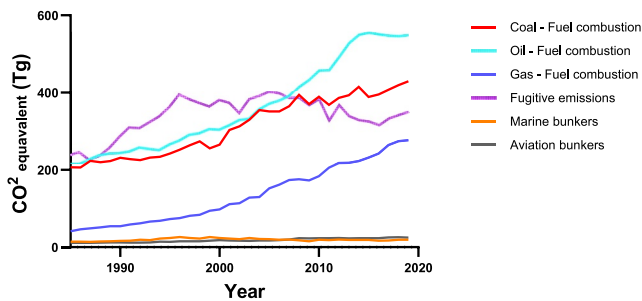


Figure 9. Fossil fuel (and biofuel) emissions by fuel type.

the RECCAP2 period, however, Africa's wood carbon imports exceeded the exports, although the amount of carbon entering the region was still relatively small in contrast to global carbon trade.

## 2.6. Anthropogenic Emissions of Greenhouse Gases From Inventory Data

We summarize the GHG emission estimates provided by the UNFCCC and International Energy Agency acquired through Climate Watch (2022). Total fossil fuel emissions increased from 1.23 PgCO<sub>2</sub>-eq to 1.74 PgCO<sub>2</sub>-eq from the 1990–2009 to 2010–2019 period (Table 11). Fossil fuel emissions contributed 42% of the total anthropogenic emissions, while LUC contributed about 32% during RECCAP2. We therefore notice that

the proportional contribution of fossil fuel emissions has increased since RECCAP1 (39% and 35% contribution for fossil fuels and LUC, respectively). Of the 23% contribution of agriculture (including livestock) to the total emissions, methane emissions are responsible for 15%. Waste includes the national reported data of solid waste disposal, wastewater treatment and discharge, and the incineration and open burning of waste as per the IPCC guidelines. Emissions reported here for Agriculture include those from enteric fermentation, manure management, agricultural soils, prescribed burning of savannas, and field burning of agricultural residues. For a comprehensive analysis and comparison of inventory data to atmospheric inversions for Africa, see Mostefaoui et al. (2024).

### 2.6.1. Emissions From Different Fossil Fuel Energy Sources

We used the Greenhouse Gas from Energy Database Highlights data set (IEA, 2023) to evaluate the greenhouse gas emissions from different energy sources (Figure 9). The data in Table 12 show that fuel combustion from coal, gas and oil increased substantially from 1985 to 2009 to 2010–2019 while the increasing trend for fugitive emissions seems to slow down for the RECCAP2 period but still contributing almost the same amount of emissions as for RECCAP1. Emissions from bunkers add a relatively small amount of emissions to the total estimate, with emissions increasing for aviation bunkers and decreasing for marine bunkers from 1985 to 2008 to 2009–2019.

## 2.7. Results of Top-Down Atmospheric Inversions

### 2.7.1. CO<sub>2</sub> Inversions

For the land CO<sub>2</sub> fluxes, we used a set of four CO<sub>2</sub> inversions that used data from the global surface in situ network: CAMS v20r2 (Chevallier et al., 2005, 2019), sEXTocNEET\_v2021 (Rödenbeck et al., 2003, 2018), Carbon Tracker Europe CTE2021 (Van Der Laan-Luijkx et al., 2017), University of Edinburgh or UoE (L. Feng et al., 2016) and one inversion driven by both in-situ and satellite column-averaged dry air mole fraction of atmospheric CO<sub>2</sub> from OCO-2 and GOSAT: CMS-Flux (J. Liu et al., 2021), all with different priors, algorithms and transport and re-analyses fields, described in the global carbon budget 2021 (Friedlingstein et al., 2022) (Figure 10). Inversions were all adjusted for fossil fuels, cement and river fluxes (see GCB—Friedlingstein et al., 2022).

Previous synthesis studies showed that the net terrestrial carbon balance of Africa is a small CO<sub>2</sub> sink (Ciais et al., 2011; Valentini et al., 2014; Williams et al., 2007). However, the inversions are subject to large uncertainties, especially in the tropics, because of the lack of observations and the difficulties of representing tropical convection and related vertical mixing (Gaubert et al., 2019; Schuh et al., 2019). Using satellite CO<sub>2</sub> column retrievals (Palmer et al., 2019) identified northern tropical Africa as being responsible for the majority of the pan-tropical net carbon seasonal cycle, with the largest emissions found over western Ethiopia and western tropical Africa during March and April.

In RECCAP1, the spread of the net exchange carbon according to four inversions was 1 PgC yr<sup>-1</sup> for five years' annual means (2001–2004). Based on

**Table 12**  
Emission Estimates (TgCO<sub>2</sub>-Eq yr<sup>-1</sup>) for Different Fossil Fuel Energy Sources

Energy source	1985–2009	2010–2019
Coal - Fuel combustion	276.51 ± 59.43	399.06 ± 18.29
Oil - Fuel combustion	298.85 ± 62.37	522.65 ± 38.78
Gas - Fuel combustion	95.03 ± 44.38	233.78 ± 30.50
Fugitive emissions	337.91 ± 57.02	340.63 ± 20.10
Marine bunkers (CO <sub>2</sub> only)	19.65 ± 3.91	18.55 ± 0.97
Aviation bunkers (CO <sub>2</sub> only)	15.34 ± 3.50	23.85 ± 1.01

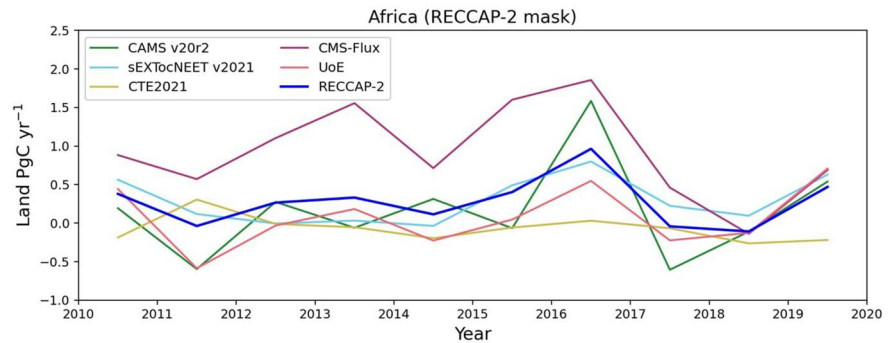


**Figure 10.** Annual land CO<sub>2</sub> fluxes (represented as year +0.5) over Africa (PgC yr<sup>−1</sup>).

our collected CO<sub>2</sub> inversions, the standard deviation was 0.25 PgC yr<sup>−1</sup> for both 2001–2004 and for 2000–2009, and 0.30 PgC yr<sup>−1</sup> for 2010–2019 (Table 13). For the 2000–2009 period, the average land flux (sink) was  $-0.14 \text{ PgC yr}^{-1} \pm 0.25 \text{ PgC yr}^{-1}$  with three out of four inversions showing moderate CO<sub>2</sub> uptake throughout the decade. In contrast, the same four inversion models find the 2010–2019 period to be a carbon source ( $0.11 \pm 0.27 \text{ PgC yr}^{-1}$ ) to the atmosphere, likely as a result of the 2015/2016 El-Niño with most inversions showing a net source in 2016 with an average flux of  $1 \text{ PgC yr}^{-1}$  (Table 13). This source is in line with previous studies that identify increased respiration rates associated with the increased surface-temperature in 2016 (Gloor et al., 2018; J. Liu et al., 2017). For the full set of five available inversion models used for the 2009–2019 period, this source is estimated at  $0.27 \pm 0.3 \text{ PgC yr}^{-1}$  as the CMS-flux inversion model estimates net emissions over most of this period. Within Africa, this source is mostly driven by emissions from the sub-humid savanna ( $0.27 \pm 0.19 \text{ PgC yr}^{-1}$ ). The CMS-Flux inversion is driven by GOSAT and OCO-2 data and shows a larger source than the in situ inversions alone. This source is driven by satellite observations of high CO<sub>2</sub> over northern tropical Africa during the dry season and might be overestimated (Gaubert et al., 2023).

### 2.7.2. CH<sub>4</sub> and N<sub>2</sub>O Inversions

We present an inter-comparison of six surface-based atmospheric inversion models for CH<sub>4</sub> over Africa and four inversions with assimilation of GOSAT observations with different transport models and inversion techniques CT-CH<sub>4</sub>/SURF (Tsuruta et al., 2017), NICAM-TM/4DVar (Niwa et al., 2017), NIES-TM-FLEXPART (Maksyutov et al., 2021; F. Wang et al., 2019), TM5-CAMS (Bergamaschi et al., 2010, 2013; Pandey et al., 2016; Segers & Houweling, 2018), TM5-4DVAR (Bergamaschi et al., 2013, 2018). The comparison reveals a significant model estimate range difference of over  $15 \text{ TgCH}_4 \text{ yr}^{-1}$  in annual mean estimates for Southern Africa (Table 14). The inversion results from surface based ensemble mean estimates for North Africa between 2009 and 2017 was  $25.94 \pm 3.03 \text{ TgCH}_4 \text{ yr}^{-1}$ , and for Southern Africa, it was  $52.08 \pm 5.05 \text{ TgCH}_4 \text{ yr}^{-1}$  (Table 14). These

**Table 13**

*Inverse Model Ensemble Summary of Posterior Land Fluxes for CO<sub>2</sub> (PgC yr<sup>−1</sup>)*

	2000–2009 (4 inversions)			2010–2019 (4 inversions)			2010–2019 (5 inversions)		
	Mean	Stdev	Range	Mean	Stdev	Range	Mean	Stdev	Range
African continent	−0.14	0.25	−0.35/0.37	0.11	0.27	−0.07/0.29	0.27	0.3	−0.07/0.93
Desert/Shrubland	0	0	−0.01/0.	0	0	−0.01/0.01	0	0	−0.01/0.01
Forest	−0.05	0.05	−0.13/0.07	−0.03	0.07	−0.16/0.06	−0.05	0.06	−0.16/0.06
North-Africa desert	0	0.01	−0.04/0.02	−0.01	0.01	−0.04/0.01	−0.01	0.01	−0.04/0.01
Semi-arid savanna	−0.03	0.05	−0.07/0.01	0.05	0.06	−0.01/0.15	0.07	0.06	−0.01/0.15
Sub-humid savanna	−0.06	0.16	−0.23/0.29	0.09	0.15	−0.1/0.25	0.27	0.19	−0.1/0.98

*Note.* A positive value means a source to the atmosphere. Value for 2009–2019 for all five available inversions are also shown (column 3), but for assessing change since the previous decade it is more appropriate to compare data with only 4 inversions.

**Table 14**  
*Inversion Estimates Include the Model Means, Variance, and Ranges for CH<sub>4</sub> and N<sub>2</sub>O*

CH <sub>4</sub> (6 surface-based inversions)	2000–2008			2009–2017		
	Mean	Model variance	Range	Mean	Model variance	Range
Africa	72.39	2.91	68.56–75.53	78.02	3.88	73.04–82.90
North Africa	23.02	3.76	19.01–27.84	25.94	3.03	22.86–30.25
Southern Africa	49.37	3.81	45.56–54.99	52.08	5.05	45.73–60.03
CH <sub>4</sub> (GOSAT inversions)	2000–2008			2009–2017		
	Mean	Model variance	Range	Mean	Model variance	Range
Africa	–	–	–	80.80	6.45	73.16–87.11
North Africa	–	–	–	23.14	2.29	21.20–26.34
Southern Africa	–	–	–	57.66	5.68	51.31–63.85
N <sub>2</sub> O	2000–2008			2009–2016		
	Mean	Model variance	Range	Mean	Model variance	Range
TgN	3.26	0.19	3.40–3.53	3.44	0.14	3.29–3.61
TgN <sub>2</sub> O	5.1182	0.2983	5.338–5.5421	5.4008	0.2198	5.1653–5.6677

values are slightly larger than the mean methane emissions during the previous period 2000–2008, which were  $23.02 \pm 3.76$  TgCH<sub>4</sub> yr<sup>−1</sup> for North Africa, and  $49.37 \pm 3.81$  TgCH<sub>4</sub> yr<sup>−1</sup> for Southern Africa. This is nearly 5% for North Africa and 12% for Southern Africa of the global total methane estimate of 557 TgCH<sub>4</sub> yr<sup>−1</sup> (F. Wang et al., 2019).

GOSAT based inversions show similar estimates to the surfacebased inversions. Mean estimates of four GOSAT-based inversions were  $23.14 \pm 2.29$  TgCH<sub>4</sub> yr<sup>−1</sup> for Northern Africa, and  $57.66 \pm 5.68$  TgCH<sub>4</sub> yr<sup>−1</sup> for Southern Africa for the years 2010–2017 (Table 14). Although Africa's contribution to global methane emissions is relatively small, it is important to monitor the continent's emissions as they may increase in the future due to population growth, urbanization, and the development of oil and gas production. Agriculture and wetlands are responsible for more than 80% of net methane emissions in Africa.

The spatial mean estimations of N<sub>2</sub>O concentrations in Africa, as reported by five inversion models, have shown a relatively small discrepancy with a mean value of  $3.26 \pm 0.19$  TgN yr<sup>−1</sup> during the years from 2000 to 2008 (Table 14). This value has slightly increased to  $3.44 \pm 0.14$  TgN yr<sup>−1</sup> from 2009 to 2016. The data from these models showed similar results over these two time periods, with a small increase in the average N<sub>2</sub>O concentrations.

### 3. Synthesis of the African Region Greenhouse Gases Budget

We summarized the estimates and trends for the African GHG flux components and carbon stocks for the RECCAP2 period (Table 15). We present separate total estimates for each of the gases (CO<sub>2</sub>, CH<sub>4</sub>, N<sub>2</sub>O) and calculated the Carbon (Pg C yr<sup>−1</sup>) and GHG budgets in CO<sub>2</sub> equivalents using the GWP100 values from the IPCC sixth assessment (IPCC, 2021). We employed both bottom-up (BU) and top-down (TD) approaches as described by Ciais et al. (2022) and compare these estimates below. Uncertainty estimates, calculated as the 5th and 95th percentiles, are provided in brackets where possible. Uncertainty in the net fluxes was difficult to calculate as some flux estimates were reported with standard deviations and other flux estimates only had minimum (min) and maximum (max) values (or 5th and 95th quantiles). For this reason, we converted all standard deviations to a 5th and 95th quantiles using the equations; min = mean − 1.645 \* sd; max = mean + 1.645 \* sd. We then produced a min and max net flux estimate by summing across these min and max values. When summing across positive and negative fluxes, we summed the smallest fluxes and not the smallest numbers. For example, if the min NPP estimate was −8.18 and the max NPP estimate was −17.44 PgC, and the min Rh was 4.8 and the max Rh was 17.2, we summed −8.18 and 4.8 and −17.44 and 17.2. This is still a very crude way of assessing uncertainty and

**Table 15**

*Synthesis of the Estimates (With Uncertainties) and Trends of GHG and Carbon Stocks (Pg) and Fluxes (Pg yr<sup>-1</sup>) for Africa Over the RECCAP2 Period (Specific Periods Depicted by Footnotes)*

Carbon stocks	CO <sub>2</sub>	CH <sub>4</sub>	N <sub>2</sub> O	Carbon budget		GHG budget (CO <sub>2</sub> equivalents)	
				Estimate (PgC)	Trend (PgC yr <sup>−1</sup> )		
Above ground biomass							
Satellite based models <sup>a</sup>				<b>84</b> <b>(71/95)</b>			
TRENDY model ensemble <sup>a</sup>				56 (48/64)			
aDGVM <sup>b</sup>				59.54			
Belowground biomass: Peat				36.9	−0.012		
Belowground biomass: Soils							
Soilgrids <sup>c</sup>				<b>87.7</b> <b>(77/99)</b>			
TRENDY model ensemble <sup>a</sup>				148 ± 60			
aDGVM <sup>b</sup>				76.77			
Total Carbon stocks				208.6			
GHG fluxes	Estimate (PgCO <sub>2</sub> yr <sup>−1</sup> )	Estimate (TgCH <sub>4</sub> yr <sup>−1</sup> )	Estimate (TgN <sub>2</sub> O yr <sup>−1</sup> )	Estimate (PgC yr <sup>−1</sup> )	Trend (PgC yr <sup>−1</sup> )	Estimate (PgCO <sub>2</sub> eq yr <sup>−1</sup> )	Trend (TgCO <sub>2</sub> eq yr <sup>−1</sup> )
GPP							
Satellite based models <sup>d</sup>	−90.5 ± 9 (−105.3/−75.6)			−24.7 ± 2.5 (−28.7/−20.6)	−0.03	−90.5 (−105.3/−75.6)	−0.12
TRENDY model ensemble <sup>a</sup>	−103.0 ± 12.4 (−123.5/−82.6)			−28.1 ± 3.4 (−33.7/−22.5)	−0.09	−103.0 (−123.5/−82.6)	−0.35
aDGVM <sup>b</sup>	−49.2 (−49.2/−49.2)			−13.4 (−13.4/−13.4)	−0.11	−49.2 (−49.2/−49.2)	−0.42
Autotrophic respiration (Ra)							
TRENDY model ensemble <sup>a</sup>	56.1 ± 9.9 (39.7/72.4)			15.3 ± 2.7 (10.8/19.8)	0.05	56.1 (39.7/72.4)	0.19
aDGVM <sup>b</sup>	4.4 (4.4/4.4)			1.2 (1.2/1.2)	0.02	4.4 (4.4/4.4)	0.06
NPP							
TRENDY model ensemble <sup>a</sup>	<b>−47.0 ± 10.3</b> <b>(−63.9/−30)</b>			<b>−12.8 ± 2.8</b> <b>(−17.4/−8.2)</b>	<b>−0.04</b>	<b>−47</b> <b>(−63.9/−30.0)</b>	<b>−0.16</b>
aDGVM <sup>b</sup>	−44.8 (−44.8/−44.8)			−12.2 (−12.2/−12.2)	−0.06	−44.8 (−44.8/−44.8)	−0.23
Heterotrophic respiration (Rh)							
TRENDY model ensemble <sup>a</sup>	<b>40.4 ± 13.9</b> <b>(17.6/63.2)</b>			<b>11.0 ± 3.8</b> <b>(4.8/17.2)</b>	<b>0.03</b>	<b>40.4</b> <b>(17.6/63.2)</b>	<b>0.09</b>
aDGVM <sup>b</sup>	32.3 (32.3/32.3)			8.8 (8.8/8.8)	0.05	32.3 (32.3/32.3)	0.19
Wild fire emissions							
FREMv2.1 <sup>a</sup>	<b>3.2</b> <b>(3.2/5.5)</b>	<b>6.8</b> <b>(4.9/9.1)</b>	<b>0.08</b> <b>(0.08/0.42)</b>	<b>1.0 ± 0.1</b> <b>(1.0/1.6)</b>	<b>−0.01</b>	<b>3.5</b> <b>(3.5/5.8)</b>	
TRENDY model ensemble <sup>a</sup>	3.2 ± 2.1 (−0.3/6.6)			0.9 ± 0.6 (−0.1/1.8)	−0.002	3.2 (−0.3/6.6)	
aDGVM <sup>b</sup>	4.2			1.2 (1.2/1.2)		4.2	



**Table 15**  
*Continued*

GHG fluxes	Estimate (PgCO <sub>2</sub> yr <sup>-1</sup> )	Estimate (TgCH <sub>4</sub> yr <sup>-1</sup> )	Estimate (TgN <sub>2</sub> O yr <sup>-1</sup> )	Estimate (PgC yr <sup>-1</sup> )	Trend (PgC yr <sup>-1</sup> )	Estimate (PgCO <sub>2</sub> eq yr <sup>-1</sup> )	Trend (TgCO <sub>2</sub> eq yr <sup>-1</sup> )
Land use change emissions							
TRENDY model ensemble <sup>a</sup>	<b>1.7 ± 0.6</b> <b>(0.8/2.7)</b>			<b>0.5 ± 0.2</b> <b>(0.2/0.7)</b>		<b>1.7</b> <b>(0.8/2.7)</b>	
Net ecosystem production	−1.5 (−4.2/3.4)	6.8 (4.9/9.1)	0.08 (0.08/0.42)	−0.35 (−1.05/1)		−1.3 (−3.9/3.5)	
Biofuel emissions <sup>a</sup>	0.9 ± 0.2 (0.6/1.2)			0.2 ± 0.05 (0.2/0.3)	0.01	0.9 (0.6/1.2)	
Crop trade fluxes <sup>a</sup>	0.1 ± 0.05 (0.03/0.19)			0.03 ± 0.01 (0.01/0.05)		0.1 (0.03/0.2)	
Wood trade fluxes <sup>a</sup>	0 ± 0.005 (−0.008/0.008)			0 ± 0.001 (−0.002/0.002)		0 (−0.008/0.008)	
Lateral fluxes (aquatic) <sup>a</sup>	−0.19 (−0.19/−0.65)			−0.05 (−0.05/−0.18)		−0.19 (−0.19/−0.65)	
Aquatic atmospheric fluxes <sup>a</sup>	1.11 (0.87/1.35)	9 (7.4/11)	0.03 (0.02/0.03)	0.31 (0.25/0.37)		1.36 (1.08/1.65)	
Organic C burial <sup>a</sup> (freshwater/coastal)	−0.15 (−0.04/−0.23)			−0.04 (−0.01/−0.06)		−0.15 (−0.05/−0.23)	
Geological fluxes <sup>a</sup>	0.02 (0/0.03)	1.01 (1.01/1.01)		0.01 (0.002/0.01)		0.05 (0.03/0.06)	
Termites <sup>a</sup>		1.4 (1.3/1.5)		0.001 (0.001/0.001)		0.04 (0.04/0.04)	
Herbivores <sup>a</sup>		17.6 (9.2/21.7)		0.013 (0.007/0.016)		0.48 (0.25/0.59)	10.8
Emissions from soil <sup>c</sup>		−1.5 ± 3 (−6.4/3.5)	1.1 ± 0.9 (−0.4/2.6)				
Net ecosystem exchange	0.3 (−2.4/4.7)	34.4 (17.3/47.7)	1.24 (−0.25/3.07)	0.16 (−0.52/1.36)		1.5 (−0.2/5.1)	
Fossil fuels <sup>a</sup>	1.28 ± 0.11 (1.1/1.45)	14.2 ± 0.8 (12.9/15.5)	0.30 ± 0 (0.29/0.31)	0.36 ± 0.03 (0.31/0.41)		1.74 (1.53/1.96)	
Bunkers <sup>a</sup>	0.04 ± 0.002 (0.04/0.04)	0.001 ± 0 (0.001/0.001)	0.001 ± 0 (0.001/0.001)	0.01 ± 0 (0.01/0.01)		0.04 (0.04/0.04)	
Agriculture <sup>a</sup>		22.5 ± 1.1 (20.7/24.2)	1.33 ± 0.04 (1.26/1.41)	0.02 ± 0 (0.02/0.02)		1.0 (0.97/1.04)	
Waste <sup>a</sup>		6.0 ± 0.3 (5.4/6.5)	0.07 ± 0.004 (0.06/0.07)	0.004 (0.004/0.005)		0.18 (0.16/0.2)	
Net bottom-up total (NBP)	1.6 (−0.9/5.8)	77 ± 2.2 (56.4/93.9)	2.9 ± 0.1 (1.4/4.9)	0.6 ± 0.2 (−0.1/1.7)		4.5 (−3.3/14.1)	
Atmospheric inversions (top-down)	0.4 (−0.26/1.06) <sup>a</sup>	78.02 ± 3.88 (73.04/82.9) <sup>f</sup>	5.40 ± 0.22 (5.17/5.67) <sup>g</sup>	0.17 ± 0.27 (−0.02/1.62)		4.0 (3.1/4.9)	

Note. Estimate units for CH<sub>4</sub> and N<sub>2</sub>O in blue italics are Tg yr<sup>-1</sup>. Where more than one estimate is provided for a component the value considered as the “best estimate” was used for calculating the net balances and is provided in bold. <sup>a</sup>2010–2019. <sup>b</sup>2009–2018. <sup>c</sup>2009–2019. <sup>d</sup>2009–2015. <sup>e</sup>Valentini et al. (2014). <sup>f</sup>2009–2017. <sup>g</sup>2009–2016.

results in very large uncertainty values, but until we have more data on all fluxes, it is the best uncertainty estimates we are able to provide at present.

Total CH<sub>4</sub> fluxes for Africa over the RECCAP2 period amount to 77 ± 2.2 (56.4/93.9) Tg C yr<sup>-1</sup>. This BU estimate is very close to the TD estimate of 78.02 ± 3.88 (73.04/82.9) from the atmospheric inversion models. An estimate of 66 ± 35 TgCH<sub>4</sub> yr<sup>-1</sup> was reported for RECCAP1 (Valentini et al., 2014). For N<sub>2</sub>O, the RECCAP2 BU estimate of 2.9 ± 0.1 (1.4/4.9) TgN<sub>2</sub>O<sup>-1</sup> is much lower than the estimate from the atmospheric inversions at

$5.401 \pm 0.22$  (5.165/5.668). The RECCAP1 estimate was  $3.3 \pm 1.3$  TgN<sub>2</sub>O yr<sup>-1</sup>. As the large majority of N<sub>2</sub>O emissions for Africa are from agricultural sources, we would expect this flux to be increasing over time. Given the lack of certain component fluxes in our bottom-up estimates and the large uncertainty associated with our estimates, a considerable effort should be directed at improving observations and estimates for CH<sub>4</sub> and N<sub>2</sub>O fluxes in Africa.

Considering the carbon in CO<sub>2</sub> and CH<sub>4</sub>, we find that the BU approach estimates Africa to contribute  $0.6 \pm 0.2$  ( $-0.1/1.7$ ) PgC yr<sup>-1</sup> to the global carbon cycle when we include non-terrestrial fluxes such as fossil fuels. Within this BU net carbon balance, terrestrial fluxes contribute  $0.16$  ( $-0.52/1.36$ ) PgC yr<sup>-1</sup> with the rest being produced through anthropogenic emissions from fossil fuels, agriculture and waste. However, the TD approaches estimate a much lower African contribution at  $0.17 \pm 0.27$  ( $-0.02/1.62$ ). Similarly, the calculated balance of fluxes from all three gases (in CO<sub>2</sub> equivalents) adds to a total of  $4.5$  ( $-3.3/14.1$ ) PgCO<sub>2</sub>eq yr<sup>-1</sup> of which NEE contributes  $1.5$  ( $-0.2/5.1$ ) PgCO<sub>2</sub>eq yr<sup>-1</sup> for the BU approaches. The TD approaches estimate the African contribution of GHG emissions at  $3.98$  (3.13/4.85) PgCO<sub>2</sub>eq yr<sup>-1</sup>. The estimate for RECCAP1 (Valentini et al., 2014) was  $-2.7 \pm 4.3$ , but they did not include key aquatic fluxes which make significant contributions. The differences between the estimates from the BU and TD approaches are not unexpected as BU approaches often omit some flux components due to the challenges in observation and lack of data. In particular, the coastal ocean margin sink (Kwon et al., 2021) could not accurately be quantified and was omitted from the final budget, and models of above and below ground biomass change require further validation. The large uncertainty values of the TD approaches are also a consequence of the sparse surface observations, which makes it difficult to constrain the inversion models.

Nevertheless, we find increasing trends of carbon and GHG emissions in the net balance estimates from both BU and TD approaches. Given the large uncertainties associated with these balances, it is difficult to definitively state that Africa is a source of carbon emissions, although it does appear to be likely. If we consider the contribution of N<sub>2</sub>O and CH<sub>4</sub> in the total GHG net emission estimate, Africa does however categorize as a net source. Certainly, we do see that Africa's carbon and GHG budget remains close to carbon neutral and still contributes a small percentage to the global budget relative to other regions. However, it is concerning that the sink capacity in Africa is decreasing.

#### 4. Conclusion

For the RECCAP2 synthesis, it is important to highlight the advances in several component estimates since the RECCAP1 period. Particularly, we incorporated the most recent methodology for biomass estimation through the use of novel L-VOD passive microwave data (Diouf et al., 2015) and LiDAR-based biomass data (Potapov et al., 2021). Fire emission estimates were improved through the use of a top-down regional product (FREMv2.1) derived specifically for Africa. Empirical data from the continent on livestock emission factors were used to adjust the livestock methane flux estimates, while new termite biomass data and emission factors shed more light on methane emissions from insects. Peatland loss rates are reported for the first time in the African GHG budget and we expect further development on this topic in the near future.

We also made a concerted attempt to calculate lateral fluxes, both from crop and wood trade, and from rivers. However, much of the data is based on coarse methods that used Tier 1 inventory data and/or taken from global models with insufficient Africa-specific observation data. Although lateral trade fluxes represent a relatively small contribution to the net estimates, future efforts should be directed at improved methodology and the inclusion of embodied carbon in products. Similarly, for carbon transport in rivers, we advocate for increased observations and empirical studies that are specific to Africa.

The information from this African budget is key to assessing which aspects of the greenhouse gas cycle are most important to be managed, and what sorts of management are possible in the quest to achieve net zero. Our budget indicates that shifts to C-neutral energy sources can potentially remove up to 30% ( $1.74$  ( $1.53/1.96$ ) PgCO<sub>2</sub>eq yr<sup>-1</sup>) of the current anthropogenic emissions, but emissions from LUC ( $1.7$  ( $0.8/2.7$ ) PgCO<sub>2</sub>eq yr<sup>-1</sup>) are more difficult to reduce. Both agricultural intensification, and expansion of agricultural land will continue to increase GHG fluxes in the short term, and the impact on the GHG budget depends on the degree to which climate-smart agricultural practices can be rolled out. This key component requires more direct attention because even with the availability of novel state-of-the-art satellite products, categorization of land use and land cover is still coarse, irregular and difficult to verify (Tubiello et al., 2023).

As natural ecosystems are increasing their C-sink capacity, and currently more than compensating for the LUC emissions ( $\text{CO}_2$  fertilization estimated as  $-2.02 + -0.88 \text{ PgCO}_2\text{eq yr}^{-1}$  by the TRENDY model ensemble), there is hope that nature-positive investments in Africa can help balance the global GHG budget. The IPCC AR6 scenarios for limiting warming to  $1.5^\circ$  include substantial carbon-capture in African ecosystems, 2.3 Pg annually by 2050, involving over 700 million ha of land (Forster et al., 2018). Key fluxes that are targeted are the fuelwood emissions ( $0.91 \text{ PgCO}_2\text{eq yr}^{-1}$ ), and the above-ground biomass (highly uncertain), as well as climate-smart agricultural practices. There is no evidence yet that this is possible within the socio-ecological context, with evidence emerging that estimates of potential above-ground biomass stocks are unrealistic, and some will have negative biodiversity and social outcomes (Armani, 2022; Bond et al., 2019). This RECCAP2 GHG budget sets a baseline against which to assess the effectiveness of policies and highlights the key fluxes that need better quantification to support financing these interventions and assessing their consequences.

Currently, the ability to accurately monitor C stock changes at large scales in Africa is limited, as the remotely sensed data sets have not been well parameterized for these ecosystems. This will improve rapidly due to private-public partnerships as C offset projects are scrutinized and verification procedures provide the motivation for improved C monitoring. Soil carbon stocks likewise, need attention in the DGVM modeling community: the TRENDY models all predict large increases in soil carbon reserves in the past few decades, but the causes of this are unclear. With better quantification, it will be easier to access funding to drive ecosystem-based mitigation activities.

A key flux highlighted here is the  $0.48 (0.248/0.585) \text{ PgCO}_2\text{eq yr}^{-1}$  contributed by livestock methane emissions. Our paper demonstrates how sensitive this value is to incorrect emissions factors and to varying livestock production systems, and highlights that there is a growing body of evidence on the continent to enable better parameterization of this important flux. It is also important to note that only 60% of this methane flux represents a net increase above what would have been emitted by the wildlife of Africa before they were replaced with livestock (Hempson et al., 2017). Options for reducing the livestock methane flux in African ecosystems need to be sensitive to the social contexts involved, but policies enabling mixed livestock-wildlife systems might prove important.

As one of the significant fluxes in Africa, fire contributed between 46% and 65% to the global fire emission estimate. We have shown that wildfire emissions decreased from the RECCAP1 period, but much of this appears to be a consequence of land conversion that manifests as an alternative source of GHG emissions to the atmosphere. Further decreases in fire emissions in Africa have been advocated to help mitigate climate change (Tear et al., 2021), but only 12% of the current emissions are considered a net source, and fire is a process that maintains functionality in a large proportion of Africa's ecosystems (e.g., grasslands and savannas).

To conclude, we show that Africa's sink capacity is decreasing and that the continent most likely switched from a small net sink to a small net source during the 2010–2019 period. Although we have improved many of the component estimates since the previous RECCAP period, we still have large uncertainties in our estimates. What is clear is that Africa has an increasing GHG emissions trend and it deviates from the mitigation aims of the Paris Agreement towards net-zero emissions. Forecasts of a growing population associated with increasing emissions from fossil fuel burning and land conversion will inevitably increase Africa's relative contribution to the global GHG estimates in the next decade. For Africa to assist with increasing international carbon trade demand from countries that are under pressure to meet their carbon dioxide reduction targets (see Jones, 2023; Yang et al., 2023), there will have to be a distinctive shift in the continents' development trajectory towards carbon-neutrality. This will require (a) enabling policy environments, (b) financial and technical support, and (c) global commitment to addressing the socio-economic challenges that will likely multiply as climate change continues to impact this region. We suggest a directed attempt to increase the GHG observation network of Africa for all BU components of the GHG budget, but especially with regard to LUC and biomass estimates. Importantly, a protocol for accountability within national pledges should be accompanied by enabling African countries to observe and report more consistently in a standardized way for centralization of data in inventories.

## Data Availability Statement

SMOS-IC L-VOD data product is available from the Centre Aval de Traitement des Données SMOS (CATDS, 2024) (<https://www.catds.fr/Products/Products-over-Land/SMOS-IC>); The X-VOD data product

(INRAE BORDEAUX Soil Moisture and VOD PRODUCTS, 2024) can be downloaded at <https://ib.remote-sensing.inrae.fr/index.php/tag/amsr2-xvod-dataset/>; GlobBiomass data and the ESA CCI (Santoro et al., 2018) biomass data is freely available for download at [https://globbiomass.org/wp-content/uploads/GB\\_Maps/Glob-biomass\\_global\\_dataset.html](https://globbiomass.org/wp-content/uploads/GB_Maps/Glob-biomass_global_dataset.html) and <https://climate.esa.int/en/projects/biomass/data/>, respectively. The NCEO product (Rodríguez-Veiga & Balzter, 2021) is available from <https://doi.org/10.25392/leicester.data.15060270.v1>; The McNicol data product (McNicol & Ryan, 2018) is available at <https://datashare.is.ed.ac.uk/handle/10283/3059>.

Soilgrids can be downloaded from <https://www.isric.org/explore/soilgrids> (Hengl et al., 2017b). The modeled GPP data derived by Tagesson et al. (2021) are available at: <https://doi.org/10.17894/ucph.b2d7ebfb-c69c-4c97-bee7-562edde5ce66> (Tagesson, 2020). TRENDY v9 simulations for the Global Carbon Budget 2020 (Friedlingstein et al., 2020b) can be obtained from [https://www.wdc-climate.de/ui/entry?acronym=DKRZ\\_LTA\\_891\\_ds00012](https://www.wdc-climate.de/ui/entry?acronym=DKRZ_LTA_891_ds00012). The HYDE database is accessible through the data portal at <https://doi.org/10.17026/dans-25g-gez3> (Klein Goldewijk, 2017). The aDGVM was forced with CCAM regionally downscaled GCM daily input data available from the Global Change Institute, University of the Witwatersrand upon request ([francois.engelbrecht@wits.ac.za](mailto:francois.engelbrecht@wits.ac.za)). The FIRE fire emissions inventory data can be provided upon request to Martin Wooster ([martin.wooster@kcl.ac.uk](mailto:martin.wooster@kcl.ac.uk)). GFED4.1 data (Randerson et al., 2017) is freely available at <https://doi.org/10.3334/ORNLDAAAC/1642>. Emission estimates from the International Energy Agency (IEA, 2022, 2023) is available at <https://www.iea.org/data-and-statistics/data-product/world-energy-statistics> and <https://www.iea.org/data-and-statistics/data-product/greenhouse-gas-emissions-from-energy-highlights>. The termite dataset and associated information (Zhou et al., 2022) are available from <https://doi.org/10.5061/dryad.vt4b8gtvk>. The gridded dataset of Etiope et al. (2018) is available for download at <https://doi.org/10.25925/4j3f-he27>. The Lacroix et al. (2020) data used to estimate fluxes from weathering are archived by the Max Planck Institute for Meteorology and are available upon request ([publications@mpimet.mpg.de](mailto:publications@mpimet.mpg.de)).

Data for inland water flux estimates are available at figshare: Lauerwald et al. (2023b) (<https://doi.org/10.6084/m9.figshare.22492504>) and <https://doi.org/10.5281/zenodo.6025626> (Borges, Deirmendjian, Bouillon, & Morana, 2022). DOC and POC estimates were based on data extracted from Zscheischler et al. (2017) and data on freshwater OC burial is available as a supplementary file to Mendonça et al. (2017). Data used for the coastal margin C input estimates as well as data for the atmospheric inversions are available from the Max Planck Institute for Biogeochemistry (2019) GeoCarbon Data Portal at <https://www.bgc-jena.mpg.de/geodb/projects/Home.php>. Estimates for crop and wood trade are based on data from the Food and Agricultural Organisation of the United Nations (FAOSTAT, 2021) available freely from <https://www.fao.org/faostat/en/#data>. Anthropogenic emission estimates presented in this paper are available from <https://www.climatewatchdata.org/> (Climate Watch, 2022).

## Acknowledgments

YE and SA were funded by the Oppenheimer Generations Research and Conservation: the Future Ecosystems for Africa Program. TT was funded by the Swedish National Space Agency (Dnr: 2021-00144; 2021-00111), FORMAS (Dnr: 2021-00644) and the EU-Aid funded CASSECS Project (Dnr: FOOD/2019/410-169). RL acknowledges funding from French state aid, managed by ANR under the “Investissements d’avenir” programme (ANR-16-CONV-0003). SL was funded by South African Research Chair Initiative (SARChI) (# 64796). CR was funded by the SECO project (Dnr: NE/T01279X/1). Nicola Stevens was funded by Trapnell Fund, Linacre College—Oxford.

## References

- Ahlström, A., Raupach, M. R., Schurgers, G., Smith, B., Arneeth, A., Jung, M., et al. (2015). The dominant role of semi-arid ecosystems in the trend and variability of the land CO<sub>2</sub> sink. *Science*, 348(6237), 895–899. <https://doi.org/10.1126/science.aaa1668>
- Ahmed, B. M., Nkunka, P. O. Y., Sileshi, G. W., French, J. R., Nyeko, P., & Jain, S. (2011). Potential impact of climate change on termite distribution in Africa. *British Journal of Environment and Climate Change*, 1(4), 172–189. <https://doi.org/10.9734/bjecc/2011/561>
- Alahacoon, N., Edirisinghe, M., Simwanda, M., Perera, E. N. C., Nyirenda, V. R., & Ranagalage, M. (2022). Rainfall variability and trends over the African continent using TAMSAT data (1983–2020): Towards climate change resilience and adaptation. *Remote Sensing*, 14(1), 1–26. <https://doi.org/10.3390/rs14010096>
- Amos (1999). *The role of wood energy in Africa*. FAO.
- Andela, N., Morton, D. C., Giglio, L., Chen, Y., van der Werf, G. R., Kasibhatla, P. S., et al. (2017). A human-driven decline in global burned area. *Science*, 356(6345), 1356–1362. <https://doi.org/10.1126/science.aal4108>
- Armani, M. A. S. Z. E. A. (2022). *Enhancing climate change adaptation and mitigation actions on land in Africa* (p. 92). Future Ecosystems for Africa (FEFA), University of the Witwatersrand. (This Work Is Licensed under Creative Commons NonCommercial, 4, 1–4)
- Avitabile, V., Herold, M., Heuvelink, G. B. M., Lewis, S. L., Phillips, O. L., Asner, G. P., et al. (2016). An integrated pan-tropical biomass map using multiple reference datasets. *Global Change Biology*, 22(4), 1406–1420. <https://doi.org/10.1111/gcb.13139>
- Baccini, A., Goetz, S. J., Walker, W. S., Laporte, N. T., Sun, M., Sulla-Menashe, D., et al. (2012). Estimated carbon dioxide emissions from tropical deforestation improved by carbon-density maps. *Nature Climate Change*, 2(3), 182–185. <https://doi.org/10.1038/nclimate1354>
- Bailis, R., Drigo, R., Ghilardi, A., & Masera, O. (2015). The carbon footprint of traditional woodfuels. *Nature Climate Change*, 5(3), 266–272. <https://doi.org/10.1038/nclimate2491>
- Bergamaschi, P., Houweling, S., Segers, A., Krol, M., Frankenberg, C., Scheepmaker, R. A., et al. (2013). Atmospheric CH<sub>4</sub> in the first decade of the 21st century: Inverse modeling analysis using SCIAMACHY satellite retrievals and NOAA surface measurements. *Journal of Geophysical Research: Atmospheres*, 118(13), 7350–7369. <https://doi.org/10.1002/jgrd.50480>

- Bergamaschi, P., Karstens, U., Manning, A. J., Saunois, M., Tsuruta, A., Berchet, A., et al. (2018). Inverse modelling of European CH<sub>4</sub> emissions during 2006–2012 using different inverse models and reassessed atmospheric observations. *Atmospheric Chemistry and Physics*, 18(2), 901–920. <https://doi.org/10.5194/acp-18-901-2018>
- Bergamaschi, P., Krol, M., Meirink, J. F., Dentener, F., Segers, A., Van Aardenne, J., et al. (2010). Inverse modeling of European CH<sub>4</sub> emissions 2001–2006. *Journal of Geophysical Research*, 115(22), 1–18. <https://doi.org/10.1029/2010JD014180>
- Blamey, R. C., Kolusu, S. R., Mahlalela, P., Todd, M. C., & Reason, C. J. C. (2018). The role of regional circulation features in regulating El Niño climate impacts over southern Africa: A comparison of the 2015/2016 drought with previous events. *International Journal of Climatology*, 38(11), 4276–4295. <https://doi.org/10.1002/joc.5668>
- Boden, T. A., Marland, G., & Andres, R. J. (2013). *Global, regional, and national fossil-fuel CO<sub>2</sub> emissions*. Oak Ridge National Laboratory, U.S. Department of Energy.
- Bombelli, A., Henry, M., Castaldi, S., Adu-Bredu, S., Arneith, A., Grandcourt, A. D., et al. (2009). The Sub-Saharan Africa carbon balance the Sub-Saharan Africa carbon balance, an overview the Sub-Saharan Africa carbon balance. Retrieved from [www.biogeosciences-discuss.net/6/2085/2009/](http://www.biogeosciences-discuss.net/6/2085/2009/)
- Bond, W. J., Stevens, N., Midgley, G. F., & Lehmann, C. E. R. (2019). The trouble with trees: Afforestation plans for Africa. *Trends in Ecology & Evolution*, 34(11), 963–965. <https://doi.org/10.1016/j.tree.2019.08.003>
- Borges, A. V., Darchambeau, F., Teodoru, C. R., Marwick, T. R., Tamooch, F., Geeraert, N., et al. (2015). Globally significant greenhouse-gas emissions from African inland waters. *Nature Geoscience*, 8(8), 637–642. <https://doi.org/10.1038/ngeo2486>
- Borges, A. V., Deirmendjian, L., Bouillon, S., & Morana, C. (2022). Data-set of CO<sub>2</sub>, CH<sub>4</sub>, N<sub>2</sub>O dissolved concentrations and ancillary data in surface waters of 24 African lakes [Dataset]. *Zenodo*. <https://doi.org/10.5281/zenodo.6025626>
- Borges, A. V., Deirmendjian, L., Bouillon, S., Okello, W., Lambert, T., Roland, F. A. E. E., et al. (2022). Greenhouse gas emissions from African lakes are no longer a blind spot. *Science Advances*, 8(25), 8716. <https://doi.org/10.1126/sciadv.abi8716>
- Bouvet, A., Mermoz, S., Le Toan, T., Villard, L., Mathieu, R., Naidoo, L., & Asner, G. P. (2018). An above-ground biomass map of African savannahs and woodlands at 25 m resolution derived from ALOS PALSAR. *Remote Sensing of Environment*, 206(November 2017), 156–173. <https://doi.org/10.1016/j.rse.2017.12.030>
- Brandt, M., Yue, Y., Wigneron, J. P., Tong, X., Tian, F., Jepsen, M. R., et al. (2018). Satellite-observed major greening and biomass increase in South China Karst during recent decade. *Earth's Future*, 6(7), 1017–1028. <https://doi.org/10.1029/2018EF000890>
- Brauman, A., Doré, J., Eggleton, P., Bignell, D., Breznak, J. A., & Kane, M. D. (2001). Molecular phylogenetic profiling of prokaryotic communities in guts of termites with different feeding habits. *FEMS Microbiology Ecology*, 35(1), 27–36. <https://doi.org/10.1111/j.1574-6941.2001.tb00785.x>
- Broadhead, J., Bahdon, J., & Whiteman, A. (2001). *Past trends and future prospects for the utilization of wood for energy (Annex 1 and Annex 2), global forest products outlook study (GFPOS)*. FAO.
- Brune, A. (2014). Symbiotic digestion of lignocellulose in termite guts. *Nature Reviews Microbiology*, 12(3), 168–180. <https://doi.org/10.1038/nrmicro3182>
- CATDS. (2024). SMOS IC products [Dataset]. *CATDS*. Retrieved from <https://www.catds.fr/Products/Products-over-Land/SMOS-IC>
- Chevallier, F., Fisher, M., Peylin, P., Serran, S., Bousquet, P., Bréon, F.-M., et al. (2005). Inferring CO<sub>2</sub> sources and sinks from satellite observations: Method and application to TOVS data. *Journal of Geophysical Research*, 110(D24), D24309. <https://doi.org/10.1029/2005JD006390>
- Chevallier, F., Remaud, M., O'Dell, C. W., Baker, D., Peylin, P., & Cozic, A. (2019). Objective evaluation of surface- and satellite-driven carbon dioxide atmospheric inversions. *Atmospheric Chemistry and Physics*, 19(22), 14233–14251. <https://doi.org/10.5194/acp-19-14233-2019>
- Ciais, P., Bastos, A., Chevallier, F., Lauerwald, R., Poulter, B., Canadell, P., et al. (2022). Definitions and methods to estimate regional land carbon fluxes for the second phase of the REgional Carbon Cycle Assessment and Processes Project (RECCAP-2). *Geoscientific Model Development*, 15(3), 1289–1316. <https://doi.org/10.5194/gmd-15-1289-2022>
- Ciais, P., Bombelli, A., Williams, M., Piao, S. L., Chave, J., Ryan, C. M., et al. (2011). The carbon balance of Africa: Synthesis of recent research studies. *Philosophical Transactions. Series A, Mathematical, Physical, and Engineering Sciences*, 369(1943), 2038–2057. <https://doi.org/10.1098/rsta.2010.0328>
- Climate Watch. (2022). Washington, DC: World Resources Institute [Dataset]. *Climate Watch*. Retrieved from <https://www.climatewatchdata.org>
- Dargie, G. C., Lewis, S. L., Lawson, I. T., Mitchard, E. T. A., Page, S. E., Bocko, Y. E., & Ifo, S. A. (2017). Age, extent and carbon storage of the central Congo Basin peatland complex. *Nature*, 542(7639), 86–90. <https://doi.org/10.1038/nature21048>
- Diouf, A. A., Brandt, M., Verger, A., El Jarroudi, M., Djaby, B., Fensholt, R., et al. (2015). Fodder biomass monitoring in Sahelian rangelands using phenological metrics from FAPAR time series. *Remote Sensing*, 7(7), 9122–9148. <https://doi.org/10.3390/rs70709122>
- Engelbrecht, F., Adegoke, J. O., Bopape, M.-J. M., Naidoo, M., Garland, R. M., Thatcher, M., et al. (2015). Projections of rapidly rising surface temperatures over Africa under low mitigation. *Environmental Research Letters*, 10(8), 085004. <https://doi.org/10.1088/1748-9326/10/8/085004>
- Ernst, Y., & Scholes, R. J. (2023). Scholes African ecoregions (version 1) [Dataset]. *Zenodo*. <https://doi.org/10.5281/zenodo.8217315>
- Etiopie, G., Ciotoli, G., Schwietzke, S., & Schoell, M. (2018). Global geological CH<sub>4</sub> emission grid files [Dataset]. *GML*. <https://doi.org/10.25925/4J3F-HE27>
- Etiopie, G., Ciotoli, G., Schwietzke, S., & Schoell, M. (2019). Gridded maps of geological methane emissions and their isotopic signature. *Earth System Science Data*, 11(1), 1–22. <https://doi.org/10.5194/essd-11-1-2019>
- FAO. (2010). Criteria and indicators for sustainable woodfuels. In *FAO forestry paper no. 160*. Rome.
- FAOSTAT. (2021). Food and agriculture statistics [Dataset]. *FAO*. Retrieved from <https://www.fao.org/faostat/en/#data>
- Feng, L., Palmer, P. I., Parker, R. J., Deutscher, N. M., Feist, D. G., Kivi, R., et al. (2016). Estimates of European uptake of CO<sub>2</sub> inferred from GOSAT XCO<sub>2</sub> retrievals: Sensitivity to measurement bias inside and outside Europe. *Atmospheric Chemistry and Physics*, 16(3), 1289–1302. <https://doi.org/10.5194/acp-16-1289-2016>
- Feng, X., Fu, B., Zhang, Y., Pan, N., Zeng, Z., Tian, H., et al. (2021). Recent leveling off of vegetation greenness and primary production reveals the increasing soil water limitations on the greening Earth. *Science Bulletin*, 66(14), 1462–1471. <https://doi.org/10.1016/j.scib.2021.02.023>
- Forster, P., Huppmann, D., Kriegler, E., Mundaca, L., Smith, C., Rogelj, J., & Séférian, R. (2018). Mitigation pathways compatible with 1.5°C in the context of sustainable development supplementary material. In V. Masson-Delmotte, P. Zhai, H.-O. Pörtner, D. Roberts, J. Skea, & P. R. Shukla (Eds.), *Global Warming of 1.5°C. An IPCC Special Report on the impacts of global warming of 1.5°C above pre-industrial levels and related global greenhouse gas emission pathways, in the context of strengthening the global response to the threat of climate change, sustainable development, and efforts to eradicate poverty*. Retrieved from <https://www.ipcc.ch/sr15>
- Friedlingstein, P., Jones, M. W., O'Sullivan, M., Andrew, R. M., Bakker, D. C. E., Hauck, J., et al. (2022). Global carbon budget 2021. *Earth System Science Data*, 14(4), 1917–2005. <https://doi.org/10.5194/essd-14-1917-2022>



- Friedlingstein, P., O'Sullivan, M., Jones, M. W., Andrew, R. M., Hauck, J., Olsen, A., et al. (2020a). Global carbon budget 2020. *Earth System Science Data*, 12(4), 3269–3340. <https://doi.org/10.5194/essd-12-3269-2020>
- Friedlingstein, P., O'Sullivan, M., Jones, M. W., Andrew, R. M., Hauck, J., Olsen, A., et al. (2020b). JSBACH 3.2 TRENDY v9 simulations for the global carbon budget 2020. *WDC*. Retrieved from [https://www.wdc-climate.de/ui/entry?acronym=DKRZ\\_LTA\\_891\\_ds00012](https://www.wdc-climate.de/ui/entry?acronym=DKRZ_LTA_891_ds00012)
- Gaubert, B., Stephens, B. B., Baker, D. F., Basu, S., Bertolacci, M., Bowman, K. W., et al. (2023). Neutral tropical African CO<sub>2</sub> exchange estimated from aircraft and satellite observations. *Global Biogeochemical Cycles*, 37(12), e2023GB007804. <https://doi.org/10.1029/2023GB007804>
- Gaubert, B., Stephens, B. B., Basu, S., Chevallier, F., Deng, F., Kort, E. A., et al. (2019). Global atmospheric CO<sub>2</sub> inverse models converging on neutral tropical land exchange, but disagreeing on fossil fuel and atmospheric growth rate. *Biogeosciences*, 16(1), 117–134. <https://doi.org/10.5194/bg-16-117-2019>
- Gilbert, M., Nicolas, G., Cinardi, G., Van Boeckel, T. P., Vanwambeke, S. O., Wint, G. R. W., & Robinson, T. P. (2018). Global distribution data for cattle, buffaloes, horses, sheep, goats, pigs, chickens and ducks in 2010. *Scientific Data*, 5, 1–11. <https://doi.org/10.1038/sdata.2018.227>
- Gloor, E., Wilson, C., Chipperfield, M. P., Chevallier, F., Buermann, W., Boesch, H., et al. (2018). Tropical land carbon cycle responses to 2015/16 El Niño as recorded by atmospheric greenhouse gas and remote sensing data. *Philosophical Transactions of the Royal Society B: Biological Sciences*, 373(1760), 20170302. <https://doi.org/10.1098/rstb.2017.0302>
- Gomes, A. L., Revermann, R., Gonçalves, F. M. P., Lages, F., Aidar, M. P. M., Sanguino Mostajo, G. A., & Finckh, M. (2021). Suffrutex grasslands in south-central Angola: Belowground biomass, root structure, soil characteristics and vegetation dynamics of the 'underground forests of africa'. *Journal of Tropical Ecology*, 37(3), 136–146. <https://doi.org/10.1017/S0266467421000298>
- Goopy, J. P., Ndung'u, P. W., Onyango, A., Kirui, P., & Butterbach-Bahl, K. (2021). Calculation of new enteric methane emission factors for small ruminants in western Kenya highlights the heterogeneity of smallholder production systems. *Animal Production Science*, 61(6), 602–612. <https://doi.org/10.1071/AN19631>
- Hansis, E., Davis, S. J., & Pongratz, J. (2015). Relevance of methodological choices for accounting of land use change carbon fluxes. *Global Biogeochemical Cycles*, 29(8), 1230–1246. <https://doi.org/10.1002/2014GB004997>
- Hanson, S., Arneth, A., Harrison, S. P., Kelley, D. I., Colin Prentice, I., Rabin, S. S., et al. (2016). The status and challenge of global fire modelling. *Biogeosciences*, 13(11), 3359–3375. <https://doi.org/10.5194/bg-13-3359-2016>
- Hartmann, J., Jansen, N., Dürr, H. H., Kempe, S., & Köhler, P. (2009). Global CO<sub>2</sub>-consumption by chemical weathering: What is the contribution of highly active weathering regions? *Global and Planetary Change*, 69(4), 185–194. <https://doi.org/10.1016/j.gloplacha.2009.07.007>
- Hartmann, J., Lauerwald, R., & Moosdorf, N. (2014). A brief overview of the GLOBAL River chemistry database, GLORICH. *Procedia Earth and Planetary Science*, 10, 23–27. <https://doi.org/10.1016/j.proeps.2014.08.005>
- Hempson, G. P., Archibald, S., & Bond, W. J. (2017). The consequences of replacing wildlife with livestock in Africa. *Scientific Reports*, 7(1), 1–10. <https://doi.org/10.1038/s41598-017-17348-4>
- Hengl, T., Heuvelink, G. B. M., Kempen, B., Leenaars, J. G. B., Walsh, M. G., Shepherd, K. D., et al. (2015). Mapping soil properties of Africa at 25 m resolution: Random forests significantly improve current predictions. *PLoS One*, 10(6), 1–26. <https://doi.org/10.1371/journal.pone.0125814>
- Hengl, T., Mendes de Jesus, J., Heuvelink, G. B. M., Ruiperez Gonzalez, M., Kilibarda, M., Blagotić, A., et al. (2017a). SoilGrids250m: Global gridded soil information based on machine learning. *PLoS One*, 12(2), e0169748. <https://doi.org/10.1371/journal.pone.0169748>
- Hengl, T., Mendes de Jesus, J., Heuvelink, G. B. M., Ruiperez Gonzalez, M., Kilibarda, M., & Blagotić, A. (2017b). SoilGrids—Global gridded soil information [Dataset]. *ISRIC*. Retrieved from <https://maps.isric.org>
- Herrero, M., Thornton, P. K., Kruska, R., & Reid, R. S. (2008). Systems dynamics and the spatial distribution of methane emissions from African domestic ruminants to 2030. *Agriculture, Ecosystems & Environment*, 126(1), 122–137. <https://doi.org/10.1016/j.agee.2008.01.017>
- Houghton, R. A., & Nassikas, A. A. (2017). Global and regional fluxes of carbon from land use and land cover change 1850–2015. *Global Biogeochemical Cycles*, 31(3), 456–472. <https://doi.org/10.1002/2016GB005546>
- Hubau, W., Lewis, S. L., Phillips, O. L., Affum-Baffoe, K., Beekman, H., Cuní-Sánchez, A., et al. (2020). Asynchronous carbon sink saturation in African and Amazonian tropical forests. *Nature*, 579(7797), 80–87. <https://doi.org/10.1038/s41586-020-2035-0>
- Hunt, J. A., Zafu, A., Mather, T. A., Pyle, D. M., & Barry, P. H. (2017). Spatially variable CO<sub>2</sub> degassing in the main Ethiopian rift: Implications for magma storage, volatile transport, and rift-related emissions. *Geochemistry, Geophysics, Geosystems*, 18(10), 3714–3737. <https://doi.org/10.1002/2017GC006975>
- IEA. (2020). *Key world energy statistics 2020*. IEA. Retrieved from <https://www.iea.org/reports/key-world-energy-statistics-2020>
- IEA. (2022). World energy statistics [Dataset]. IEA. Retrieved from <https://www.iea.org/data-and-statistics/data-product/world-energy-statistics>
- IEA. (2023). Greenhouse gas emissions from energy highlights [Dataset]. IEA. Retrieved from <https://www.iea.org/data-and-statistics/data-product/greenhouse-gas-emissions-from-energy-highlights>
- INRAE BORDEAUX Soil Moisture and VOD PRODUCTS. (2024). AMSR2 IB X-VOD [Dataset]. INRAE. Retrieved from <https://ib.remote-sensing.inrae.fr/index.php/tag/amr2-xvod-dataset/>
- IPCC. (2006). IPCC guidelines for national greenhouse gas inventories. In H. S. Eggleston, L. Buendia, K. Miwa, T. Ngara, & K. Tanabe (Eds.), *Prepared by the national greenhouse gas inventories programme*. IGES, Japan.
- IPCC. (2019). Volume 4: Agriculture, forestry and other land use. In *Chapter 10: Emissions from livestock and manure management. 2019 refinement to the 2006 IPCC guidelines for national greenhouse gas inventories* (Vol. 4, p. 209).
- IPCC. (2021). Climate change 2021: The physical science basis. In V. Masson-Delmotte, P. Zhai, A. Pirani, S. L. Connors, C. Péan, et al. (Eds.), *Contribution of working group I to the sixth assessment report of the intergovernmental panel on climate change*. Cambridge University Press. <https://doi.org/10.1017/9781009157896>
- Jones, C. D. (2023). Burden sharing for CDR: Balancing fair liability with feasibility. *National Science Review*, 10(12), nwad211. <https://doi.org/10.1093/nsr/nwad211>
- Joosten, H. (2009). The global peatland CO<sub>2</sub> picture, Africa (Vol. 11).
- Kirschke, S., Bousquet, P., Ciais, P., Saunio, M., Canadell, J. G., Dlugokencky, E. J., et al. (2013). Three decades of global methane sources and sinks. *Nature Geoscience*, 6(10), 813–823. <https://doi.org/10.1038/ngeo1955>
- Klein Goldewijk, C. G. M., Beusen, A., Doelman, J., & Stehfest, E. (2017). Anthropogenic land-use estimates for the Holocene, HYDE 3.2 [Dataset]. *DANS Data Station Archaeology*, VI, 9(2), 927–953. <https://doi.org/10.17026/dans-25g-gez3>
- Kwon, E. Y., DeVries, T., Galbraith, E. D., Hwang, J., Kim, G., & Timmermann, A. (2021). Stable carbon isotopes suggest large terrestrial carbon inputs to the global ocean. *Global Biogeochemical Cycles*, 35(4), 1–25. <https://doi.org/10.1029/2020GB006684>
- Lacroix, F., Ilyina, T., & Hartmann, J. (2020). Oceanic CO<sub>2</sub> outgassing and biological production hotspots induced by pre-industrial river loads of nutrients and carbon in a global modeling approach. *Biogeosciences*, 17(1), 55–88. <https://doi.org/10.5194/bg-17-55-2020>

- Lasslop, G., Hantson, S., Harrison, S. P., Bachelet, D., Burton, C., Forkel, M., et al. (2020). Global ecosystems and fire: Multi-model assessment of fire-induced tree-cover and carbon storage reduction. *Global Change Biology*, 26(9), 5027–5041. <https://doi.org/10.1111/gcb.15160>
- Lauerwald, R., Allen, G. H., Deemer, B. R., Liu, S., Maavara, T., Raymond, P., et al. (2023a). Inland water greenhouse gas budgets for RECCAP2: 2. Regionalization and homogenization of estimates. *Global Biogeochemical Cycles*, 37(5), e2022GB007658. <https://doi.org/10.1029/2022GB007658>
- Lauerwald, R., Allen, G. H., Deemer, B. R., Liu, S., Maavara, T., Raymond, P., et al. (2023b). Table S1—Rescaled and regionalized inland water greenhouse gas budgets for RECCAP-2 [Dataset]. *figshare*. <https://doi.org/10.6084/m9.figshare.22492504.v1>
- Lee, H., Muirhead, J. D., Fischer, T. P., Ebinger, C. J., Kattenhorn, S. A., Sharp, Z. D., & Kianji, G. (2016). Massive and prolonged deep carbon emissions associated with continental rifting. *Nature Geoscience*, 9(2), 145–149. <https://doi.org/10.1038/ngeo2622>
- Lewis, S. L., Lopez-Gonzalez, G., Sonké, B., Affum-Baffoe, K., Baker, T. R., Ojo, L. O., et al. (2009). Increasing carbon storage in intact African tropical forests. *Nature*, 457(7232), 1003–1006. <https://doi.org/10.1038/nature07771>
- Lickley, M., & Solomon, S. (2018). Drivers, timing and some impacts of global aridity change. *Environmental Research Letters*, 13(10), 104010. <https://doi.org/10.1088/1748-9326/aac013>
- Liu, J., Baskaran, L., Bowman, K., Schimel, D., Bloom, A. A., Parazoo, N. C., et al. (2021). Carbon monitoring system flux net biosphere exchange 2020 (CMS-Flux NBE 2020). *Earth System Science Data*, 13(2), 299–330. <https://doi.org/10.5194/essd-13-299-2021>
- Liu, J., Bowman, K. W., Schimel, D. S., Parazoo, N. C., Jiang, Z., Lee, M., et al. (2017). Contrasting carbon cycle responses of the tropical continents to the 2015–2016 El Niño. *Science*, 358(6360), eaam5690. <https://doi.org/10.1126/science.aam5690>
- Liu, Y. Y., van Dijk, A. I. J. M., de Jeu, R. A. M., Canadell, J. G., McCabe, M. F., Evans, J. P., & Wang, G. (2015). Recent reversal in loss of global terrestrial biomass. *Nature Climate Change*, 5(5), 470–474. <https://doi.org/10.1038/nclimate2581>
- Lourenco, M., Fitchett, J. M., & Woodborne, S. (2022). Angolan highlands peatlands: Extent, age and growth dynamics. *Science of the Total Environment*, 810, 152315. <https://doi.org/10.1016/j.scitotenv.2021.152315>
- Ludwig, W., Amiotte-Suchet, P., Munhoven, G., & Probst, J.-L. (1998). Atmospheric CO<sub>2</sub> consumption by continental erosion: Present-day controls and implications for the last glacial maximum. *Global and Planetary Change*, 16–17, 107–120. [https://doi.org/10.1016/S0921-8181\(98\)00016-2](https://doi.org/10.1016/S0921-8181(98)00016-2)
- Macdonald, J. A., Jeeva, D., Eggleton, P., Davies, R., Bignell, D. E., Fowler, D., et al. (1999). The effect of termite biomass and anthropogenic disturbance on the CH<sub>4</sub> budgets of tropical forests in Cameroon and Borneo. *Global Change Biology*, 5(8), 869–879. <https://doi.org/10.1046/j.1365-2486.1999.00279.x>
- Maksyutov, S., Oda, T., Saito, M., Janardanan, R., Belikov, D., Kaiser, J. W., et al. (2021). Technical note: A high-resolution inverse modelling technique for estimating surface CO<sub>2</sub> fluxes based on the NIES-TM-FLEXPART coupled transport model and its adjoint. *Atmospheric Chemistry and Physics*, 21(2), 1245–1266. <https://doi.org/10.5194/acp-21-1245-2021>
- Martens, C., Hickler, T., Davis-Reddy, C., Engelbrecht, F., Higgins, S. I., von Maltitz, G. P., et al. (2021). Large uncertainties in future biome changes in Africa call for flexible climate adaptation strategies. *Global Change Biology*, 27(2), 340–358. <https://doi.org/10.1111/gcb.15390>
- Max Planck Institute for Biogeochemistry. (2019). GeoCarbon data portal [Dataset]. *Max Planck Institute*. Retrieved from <https://www.bgc-jena.mpg.de/geodb/projects/Home.php>
- McNicol, I., & Ryan, C. (2018). Carbon losses from deforestation and widespread degradation offset by extensive growth in African woodlands, 2007–2010 [Dataset]. *University of Edinburgh. School of Geosciences*. <https://doi.org/10.7488/ds/2408>
- McNicol, I. M., Ryan, C. M., & Mitchard, E. T. A. (2018). Carbon losses from deforestation and widespread degradation offset by extensive growth in African woodlands. *Nature Communications*, 9(1), 3045. <https://doi.org/10.1038/s41467-018-05386-z>
- Mendonça, R., Müller, R. A., Clow, D., Verpoorter, C., Raymond, P., Tranvik, L. J., & Sobek, S. (2017). Organic carbon burial in global lakes and reservoirs. *Nature Communications*, 8(1), 1694. <https://doi.org/10.1038/s41467-017-01789-6>
- Mostefaoui, M., Ciais, P., McGrath, M. J., Peylin, P., Patra, P. K., & Ernst, Y. (2024). Greenhouse gas emissions and their trends over the last 3 decades across Africa. *Earth System Science Data*, 16(1), 245–275. <https://doi.org/10.5194/essd-16-245-2024>
- Ndung'u, P. W., Takahashi, T., du Toit, C. J. L., Robertson-Dean, M., Butterbach-Bahl, K., McAuliffe, G. A., et al. (2022). Farm-level emission intensities of smallholder cattle (*Bos indicus*; *B. indicus*–*B. taurus* crosses) production systems in highlands and semi-arid regions. *Animal*, 16(1), 100445. <https://doi.org/10.1016/j.animal.2021.100445>
- Nguyen, H. M., & Wooster, M. J. (2020). Remote Sensing of Environment Advances in the estimation of high Spatio-temporal resolution pan-African top-down biomass burning emissions made using geostationary fire radiative power (FRP) and MAIAC aerosol optical depth (AOD) data. *Remote Sensing of Environment*, 248(July), 111971. <https://doi.org/10.1016/j.rse.2020.111971>
- Niwa, Y., Tomita, H., Satoh, M., Imasu, R., Sawa, Y., Tsuboi, K., et al. (2017). A 4D-Var inversion system based on the icosahedral grid model (NICAM-TM 4D-Var v1.0)-Part I: Offline forward and adjoint transport models. *Geoscientific Model Development*, 10(3), 1157–1174. <https://doi.org/10.5194/gmd-10-1157-2017>
- Pachzelt, A., Forrest, M., Rammig, A., Higgins, S. I., & Hickler, T. (2015). Potential impact of large ungulate grazers on African vegetation, carbon storage and fire regimes. *Global Ecology and Biogeography*, 24(9), 991–1002. <https://doi.org/10.1111/geb.12313>
- Palmer, P. I., Feng, L., Baker, D., Chevallier, F., Bösch, H., & Somkuti, P. (2019). Net carbon emissions from African biosphere dominate pan-tropical atmospheric CO<sub>2</sub> signal. *Nature Communications*, 10(1), 1–9. <https://doi.org/10.1038/s41467-019-11097-w>
- Pan, S., Dangal, S. R. S., Tao, B., Yang, J., & Tian, H. (2015). Recent patterns of terrestrial net primary production in Africa influenced by multiple environmental changes. *Ecosystem Health and Sustainability*, 1(5), 1–15. <https://doi.org/10.1890/EHS14-0027.1>
- Pandey, S., Houweling, S., Krol, M., Aben, I., Chevallier, F., Dlugokencky, E. J., et al. (2016). Inverse modeling of GOSAT-retrieved ratios of total column CH<sub>4</sub> and CO<sub>2</sub> for 2009 and 2010. *Atmospheric Chemistry and Physics*, 16(8), 5043–5062. <https://doi.org/10.5194/acp-16-5043-2016>
- Peñuelas, J., Poulter, B., Sardans, J., Ciais, P., van der Velde, M., Bopp, L., et al. (2013). Human-induced nitrogen–phosphorus imbalances alter natural and managed ecosystems across the globe. *Nature Communications*, 4(1), 2934. <https://doi.org/10.1038/ncomms3934>
- Peters, G. P., Davis, S. J., & Andrew, R. (2012). A synthesis of carbon in international trade. *Biogeosciences*, 9(8), 3247–3276. <https://doi.org/10.5194/bg-9-3247-2012>
- Piao, S., Wang, X., Park, T., Chen, C., Lian, X., He, Y., et al. (2020). Characteristics, drivers and feedbacks of global greening. *Nature Reviews Earth & Environment*, 1(1), 14–27. <https://doi.org/10.1038/s43017-019-0001-x>
- Potapov, P., Li, X., Hernandez-Serna, A., Tyukavina, A., Hansen, M. C., Kommareddy, A., et al. (2021). Mapping global forest canopy height through integration of GEDI and Landsat data. *Remote Sensing of Environment*, 253, 1–30. <https://doi.org/10.1016/j.rse.2020.112165>
- Potapov, P., Turubanova, S., Hansen, M. C., Tyukavina, A., Zalles, V., Khan, A., et al. (2022). Global maps of cropland extent and change show accelerated cropland expansion in the twenty-first century. *Nature Food*, 3(1), 19–28. <https://doi.org/10.1038/s43016-021-00429-z>

- Ramo, R., Roteta, E., Bistinas, I., Van Wees, D., Bastarrika, A., Chuvieco, E., & Van der Werf, G. R. (2021). African burned area and fire carbon emissions are strongly impacted by small fires undetected by coarse resolution satellite data. *Proceedings of the National Academy of Sciences*, 118(9), e2011160118. <https://doi.org/10.1073/pnas.2011160118>
- Randerson, J. T., Van Der Werf, G. R., Giglio, L., Collatz, G. J., & Kasibhatla, P. S. (2017). Global fire emissions database, version 4.1 (GFEDv4). ORNL distributed active archive center. [Dataset]. *ORNL*. <https://doi.org/10.3334/ORNLDAAAC/1293>
- Räsänen, M., Vesala, R., Rönnholm, P., Arppe, L., Manninen, P., & Jylhä, M. (2023). Carbon dioxide and methane fluxes from mounds of African fungus-growing termites (pp. 4029–4042).
- Rödenbeck, C., Houweling, S., Gloor, M., & Heimann, M. (2003). CO<sub>2</sub> flux history 1982–2001 inferred from atmospheric data using a global inversion of atmospheric transport. *Atmospheric Chemistry and Physics*, 3(6), 1919–1964. <https://doi.org/10.5194/acp-3-1919-2003>
- Rödenbeck, C., Zachle, S., Keeling, R., & Heimann, M. (2018). How does the terrestrial carbon exchange respond to inter-annual climatic variations? A quantification based on atmospheric CO<sub>2</sub> data. *Biogeosciences*, 15(8), 2481–2498. <https://doi.org/10.5194/bg-15-2481-2018>
- Rodríguez-Veiga, P., & Balzter, H. (2021). NCEO africa AGB. [Dataset]. *Copernicus*. <https://doi.org/10.25392/leicester.data.15060270.v1>
- Rodríguez-Veiga, P., Wheeler, J., Louis, V., Tansey, K., & Balzter, H. (2017). Quantifying forest biomass carbon stocks from space. *Current Forestry Reports*, 3(1), 1–18. <https://doi.org/10.1007/s40725-017-0052-5>
- Roteta, E., Bastarrika, A., Padilla, M., Storm, T., & Chuvieco, E. (2019). Development of a Sentinel-2 burned area algorithm: Generation of a small fire database for sub-Saharan Africa. *Remote Sensing of Environment*, 222, 1–17. <https://doi.org/10.1016/j.rse.2018.12.011>
- Rouland, C., Brauman, A., Labat, M., & Lepage, M. (1993). Nutritional factors affecting methane emission from termites. *Chemosphere*, 26(1), 617–622. [https://doi.org/10.1016/0045-6535\(93\)90447-D](https://doi.org/10.1016/0045-6535(93)90447-D)
- Saatchi, S. S., Harris, N. L., Brown, S., Lefsky, M., Mitchard, E. T. A., Salas, W., et al. (2011). Benchmark map of forest carbon stocks in tropical regions across three continents. *Proceedings of the National Academy of Sciences*, 108(24), 9899–9904. <https://doi.org/10.1073/pnas.1019576108>
- Sankaran, M., Hanan, N. P., Scholes, R. J., Ratnam, J., Augustine, D. J., Cade, B. S., et al. (2005). Determinants of woody cover in African savannas. *Nature*, 438(7069), 846–849. <https://doi.org/10.1038/nature04070>
- Santoro, M., Cartus, O., Carvalhais, N., Rozendaal, D. M. A. A., Avitabile, V., Araza, A., et al. (2021). The global forest above-ground biomass pool for 2010 estimated from high-resolution satellite observations. *Earth System Science Data*, 13(8), 3927–3950. <https://doi.org/10.5194/essd-13-3927-2021>
- Santoro, M., Cartus, O., Mermoz, S., Bouvet, A., Le Toan, T., Carvalhais, N., et al. (2018). GlobBiomass global above-ground biomass and growing stock volume [Dataset]. *Globbiomass*. Retrieved from [https://globbiomass.org/wp-content/uploads/GB\\_Maps/Globbiomass\\_global\\_dataset.html](https://globbiomass.org/wp-content/uploads/GB_Maps/Globbiomass_global_dataset.html)
- Sato, H., & Ise, T. (2012). Effect of plant dynamic processes on African vegetation responses to climate change: Analysis using the spatially explicit individual-based dynamic global vegetation model (SEIB-DGVM). *Journal of Geophysical Research*, 117, G3. <https://doi.org/10.1029/2012JG002056>
- Saunio, M., Stavert, A. R., Poulter, B., Bousquet, P., Canadell, G., Jackson, R., et al. (2020). The global methane budget 2000–2017. *Earth System Science Data*, 12(3), 1561–1623. <https://doi.org/10.5194/essd-12-1561-2020>
- Scheiter, S., & Higgins, S. I. (2009). Impacts of climate change on the vegetation of Africa: An adaptive dynamic vegetation modelling approach. *Global Change Biology*, 15(9), 2224–2246. <https://doi.org/10.1111/j.1365-2486.2008.01838.x>
- Scholes, R. J., Archibald, S., & Maltitz, G. V. (2011). Emissions from fire in sub-Saharan Africa: The magnitude of sources, their variability and uncertainty.
- Schuh, A. E., Jacobson, A. R., Basu, S., Weir, B., Baker, D., Bowman, K., et al. (2019). Quantifying the impact of atmospheric transport uncertainty on CO<sub>2</sub> surface flux estimates. *Global Biogeochemical Cycles*, 33(4), 484–500. <https://doi.org/10.1029/2018GB006086>
- Segers, A., & Houweling, S. (2018). *Validation of the CH<sub>4</sub> surface flux inversion—Reanalysis 1990–2017*. Copernicus Atmosphere Monitoring Service.
- Song, X.-P., Hansen, M. C., Stehman, S. V., Potapov, P. V., Tyukavina, A., Vermote, E. F., & Townshend, J. R. (2018). Global land change from 1982 to 2016. *Nature*, 560(7720), 639–643. <https://doi.org/10.1038/s41586-018-0411-9>
- Stevens, N., Erasmus, B. F. N., Archibald, S., & Bond, W. J. (2016). Woody encroachment over 70 years in South African savannahs: Overgrazing, global change or extinction aftermath? *Philosophical Transactions of the Royal Society of London. Series B, Biological Sciences*, 371(1703), 20150437. <https://doi.org/10.1098/rstb.2015.0437>
- Tagesson, T., Ardö, J., Cappelaere, B., Kergoat, L., Abdi, A., Horion, S., & Fensholt, R. (2017). Modelling spatial and temporal dynamics of gross primary production in the Sahel from earth-observation-based photosynthetic capacity and quantum efficiency. *Biogeosciences*, 14(5), 1333–1348. <https://doi.org/10.5194/bg-14-1333-2017>
- Tagesson, T., Tian, F., Schurgers, G., Horion, S., Scholes, R., Ahlström, A., et al. (2021). A physiology-based Earth observation model indicates stagnation in the global gross primary production during recent decades. *Global Change Biology*, 27(4), 836–854. <https://doi.org/10.1111/gcb.15424>
- Tagesson, T. (2020). Light response function modelled gross primary production. [Dataset]. *ERDA*. <https://doi.org/10.17894/ucph.b2d7ebfb-c69c-4c97-bee7-562edde5ce66>
- Tear, T. H., Wolff, N. H., Lipsett-Moore, G. J., Ritchie, M. E., Ribeiro, N. S., Petracca, L. S., et al. (2021). Savanna fire management can generate enough carbon revenue to help restore Africa's rangelands and fill protected area funding gaps. *One Earth*, 4(12), 1776–1791. <https://doi.org/10.1016/j.oneear.2021.11.013>
- Tsuruta, A., Aalto, T., Backman, L., Hakkarainen, J., Van Der Laan-Luijckx, I. T., Krol, M. C., et al. (2017). Global methane emission estimates for 2000–2012 from CarbonTracker Europe-CH4 v1.0. *Geoscientific Model Development*, 10(3), 1261–1289. <https://doi.org/10.5194/gmd-10-1261-2017>
- Tubiello, F. N., Conchedda, G., Casse, L., Pengyu, H., Zhongxin, C., De Santis, G., et al. (2023). Measuring the world's cropland area. *Nature Food*, 4(1), 30–32. <https://doi.org/10.1038/s43016-022-00667-9>
- UNEP. (2022). *Global peatlands assessment—The state of the World's peatlands: Evidence for action toward the conservation, restoration, and sustainable management of peatlands. Main report*. Global Peatlands Initiative. United Nations Environment Programme.
- United Nations Urban Settlement Programme. (2019). *World population prospects 2019*. Department of Economic and Social Affairs. World Population Prospects 2019.
- Valentini, R., Arneeth, A., Bombelli, A., Castaldi, S., Gatti, R. C., Chevallier, F., et al. (2014). A full greenhouse gases budget of Africa: Synthesis, uncertainties, and vulnerabilities. *Biogeosciences*, 11(2), 381–407. <https://doi.org/10.5194/bg-11-381-2014>
- Van Der Laan-Luijckx, I. T., Van Der Velde, I. R., Van Der Veen, E., Tsuruta, A., Stanislawski, K., Babenhauserheide, A., et al. (2017). The CarbonTracker data assimilation Shell (CTDAS) v1.0: Implementation and global carbon balance 2001–2015. *Geoscientific Model Development*, 10(7), 2785–2800. <https://doi.org/10.5194/gmd-10-2785-2017>



- van der Werf, G. R., Guido, R., Randerson, J. T., Giglio, L., Van Leeuwen, T. T., Chen, Y., et al. (2017). Global fire emissions estimates during 1997–2016. *Earth System Science Data*, 9(2), 697–720. <https://doi.org/10.5194/essd-9-697-2017>
- Venter, Z. S., Cramer, M. D., & Hawkins, H.-J. (2018). Drivers of woody plant encroachment over Africa. *Nature Communications*, 9(1), 2272. <https://doi.org/10.1038/s41467-018-04616-8>
- Wang, F., Maksyutov, S., Tsuruta, A., Janardanan, R., Ito, A., Sasakawa, M., et al. (2019). Methane emission estimates by the global high-resolution inverse model using national inventories. *Remote Sensing*, 11(21), 1–19. <https://doi.org/10.3390/rs11212489>
- Wang, M., Wigneron, J. P., Sun, R., Fan, L., Frappart, F., Tao, S., et al. (2021). A consistent record of vegetation optical depth retrieved from the AMSR-E and AMSR2 X-band observations. *International Journal of Applied Earth Observation and Geoinformation*, 105, 102609. <https://doi.org/10.1016/j.jag.2021.102609>
- Wang, S., Zhang, Y., Ju, W., Chen, J. M., Ciais, P., Cescatti, A., et al. (2020). Recent global decline of CO<sub>2</sub> fertilization effects on vegetation photosynthesis. *Science*, 370(6522), 1295–1300. <https://doi.org/10.1126/science.abb7772>
- White, F. (1983). Vegetation of Africa—A descriptive memoir to accompany the Unesco/AETFAT/UNSO vegetation map of Africa. In *Natural Resources Research report XX; U. N. Educational, Scientific and Cultural Organization; 7 Place de Fontenay, 75700 Paris, France* (p. 356)
- Williams, C. A., Hanan, N. P., Neff, J. C., Scholes, R. J., Berry, J. A., Denning, A. S., & Baker, D. F. (2007). Africa and the global carbon cycle. *Carbon Balance and Management*, 2(1), 3. <https://doi.org/10.1186/1750-0680-2-3>
- Winkler, A. J., Myneni, R. B., Hannart, A., Sitch, S., Haverd, V., Lombardozzi, D., et al. (2021). Slowdown of the greening trend in natural vegetation with further rise in atmospheric CO<sub>2</sub>. *Biogeosciences*, 18(17), 4985–5010. <https://doi.org/10.5194/bg-18-4985-2021>
- Wolf, J., Asrar, G. R., & West, T. O. (2017). Revised methane emissions factors and spatially distributed annual carbon fluxes for global livestock. *Carbon Balance and Management*, 12(1), 16. <https://doi.org/10.1186/s13021-017-0084-y>
- Yang, P., Mi, Z., Wei, Y. M., Hanssen, S. V., Liu, L. C., Coffman, D., et al. (2023). The global mismatch between equitable carbon dioxide removal liability and capacity. *National Science Review*, 10(12), nwad254. <https://doi.org/10.1093/nsr/nwad254>
- Yuan, W., Zheng, Y., Piao, S., Ciais, P., Lombardozzi, D., Wang, Y., et al. (2019). Increased atmospheric vapor pressure deficit reduces global vegetation growth. *Science Advances*, 5(8), eaax1396. <https://doi.org/10.1126/sciadv.aax1396>
- Zheng, B., Ciais, P., Chevallier, F., Chuvieco, E., Chen, Y., & Yang, H. (2021). Increasing forest fire emissions despite the decline in global burned area. *Science Advances*, 7(39), eabh2646. <https://doi.org/10.1126/sciadv.abh2646>
- Zhou, Y., Staver, A. C., & Davies, A. B. (2023). Species-level termite methane production rates. *Ecology*, 104(2), e3905. <https://doi.org/10.1002/ecy.3905>
- Zhou, Y., Staver, C., & Davies, A. (2022). Species-level termite methane production rates [Dataset]. *Dryad*, 104(2), e3905. <https://doi.org/10.5061/dryad.vt4b8gtvk>
- Zscheischler, J., Mahecha, M. D., Avitabile, V., Calle, L., Carvalhais, N., Ciais, P., et al. (2017). Reviews and syntheses: An empirical spatio-temporal description of the global surface-atmosphere carbon fluxes: Opportunities and data limitations. *Biogeosciences*, 14(15), 3685–3703. <https://doi.org/10.5194/bg-14-3685-2017>
- Zubkova, M., Boschetti, L., Abatzoglou, J. T., & Giglio, L. (2019). Changes in fire activity in Africa from 2002 to 2016 and their potential drivers. *Geophysical Research Letters*, 46(13), 7643–7653. <https://doi.org/10.1029/2019gl083469>

## References From the Supporting Information

- Amos, S. (1999). *The role of wood energy in Africa*. FAO.
- Andreae, M. O. (2019). Emission of trace gases and aerosols from biomass burning—An updated assessment. *Atmospheric Chemistry and Physics*, 19(13), 8523–8546. <https://doi.org/10.5194/acp-19-8523-2019>
- Baccini, A., Walker, W., Carvalho, L., Farina, M., Sulla-Menashe, D., & Houghton, R. A. (2017). Tropical forests are a net carbon source based on aboveground measurements of gain and loss. *Science*, 358(6360), 230–234. <https://doi.org/10.1126/science.aam5962>
- Brümmer, C., Papen, H., Wassmann, R., & Brüggemann, N. (2009). Fluxes of CH<sub>4</sub> and CO<sub>2</sub> from soil and termite mounds in south Sudanian savanna of Burkina Faso (West Africa). *Global Biogeochemical Cycles*, 23(1). <https://doi.org/10.1029/2008GB003237>
- Goopy, J. P., Onyango, A. A., Dickhoefer, U., & Butterbach-Bahl, K. (2018). A new approach for improving emission factors for enteric methane emissions of cattle in smallholder systems of East Africa—Results for Nyando, Western Kenya. *Agricultural Systems*, 161, 72–80. <https://doi.org/10.1016/j.agsy.2017.12.004>
- Ichoku, C., & Ellison, L. (2014). Global top-down smoke-aerosol emissions estimation using satellite fire radiative power measurements. *Atmospheric Chemistry and Physics*, 14(13), 6643–6667. <https://doi.org/10.5194/acp-14-6643-2014>
- Jones, L. A., Kimball, J. S., Reichle, R. H., Madani, N., Glassy, J., Ardizzone, J. V., et al. (2017). The SMAP level 4 carbon product for monitoring ecosystem land-atmosphere CO<sub>2</sub> exchange. *IEEE Transactions on Geoscience and Remote Sensing*, 55(11), 6517–6532. <https://doi.org/10.1109/TGRS.2017.2729343>
- Jung, M., Reichstein, M., Margolis, H. A., Cescatti, A., Richardson, A. D., Arain, M. A., et al. (2011). Global patterns of land-atmosphere fluxes of carbon dioxide, latent heat, and sensible heat derived from eddy covariance, satellite, and meteorological observations. *Journal of Geophysical Research*, 116(G3), G00J07. <https://doi.org/10.1029/2010JG001566>
- Kaiser, J. W., Heil, A., Andreae, M. O., Benedetti, A., Chubarova, N., Jones, L., et al. (2012). Biomass burning emissions estimated with a global fire assimilation system based on observed fire radiative power. *Biogeosciences*, 9(1), 527–554. <https://doi.org/10.5194/bg-9-527-2012>
- Mota, B., & Wooster, M. J. (2018). A new top-down approach for directly estimating biomass burning emissions and fuel consumption rates and totals from geostationary satellite fire radiative power (FRP). *Remote Sensing of Environment*, 206, 45–62. <https://doi.org/10.1016/j.rse.2017.12.016>
- Ndung'u, P. W., Kirui, P., Takahashi, T., du Toit, C. J. L., Merbold, L., & Goopy, J. P. (2021). Data describing cattle performance and feed characteristics to calculate enteric methane emissions in smallholder livestock systems in Bomet County, Kenya. *Data in Brief*, 39, 107673. <https://doi.org/10.1016/j.dib.2021.107673>
- Nguyen, H. M., & Wooster, M. (2020). Advances in the estimation of high Spatio-temporal resolution pan-African top-down biomass burning emissions made using geostationary fire radiative power (FRP) and MAIAC aerosol optical depth (AOD) data. *Remote Sensing of Environment*, 248(November 2019), 111971. <https://doi.org/10.1016/j.rse.2020.111971>
- Nyamadzawo, G., Gotosa, J., Muvengwi, J., Wuta, M., Nyamangara, J., Nyamugafata, P., & Smith, L. J. (2012). The effect of Catena position on greenhouse gas emissions from Dambo Located termite (*Odontotermes transvaalensis*) mounds from Central Zimbabwe. *Atmospheric and Climate Sciences*, 2(4), 501–509. <https://doi.org/10.4236/acs.2012.24044>
- Ochiai, O., Poulter, B., Seifert, F. M., Ward, S., Jarvis, I., Whitcraft, A., et al. (2023). iScience II towards a roadmap for space-based observations of the land sector for the UNFCCC global stocktake. *ISCIENCE*, 26(4), 106489. <https://doi.org/10.1016/j.isci.2023.106489>

- Pelletier, J., Paquette, A., Mbindo, K., Zimba, N., Siampale, A., Chendauka, B., et al. (2018). Carbon sink despite large deforestation in African tropical dry forests (miombo woodlands). *Environmental Research Letters*, 13(9), 94017. <https://doi.org/10.1088/1748-9326/aadc9a>
- Potapov, P., Hansen, M. C., Pickens, A., Hernandez-Serna, A., Tyukavina, A., Turubanova, S., et al. (2022). The global 2000–2020 land cover and land Use change dataset derived from the Landsat archive: First results. *Frontiers in Remote Sensing*, 3(April), 1–22. <https://doi.org/10.3389/frsen.2022.856903>
- Poulter, B., Frank, D. C., Hodson, E. L., & Zimmermann, N. E. (2011). Impacts of land cover and climate data selection on understanding terrestrial carbon dynamics and the CO<sub>2</sub> airborne fraction. *Biogeosciences*, 8(8), 2027–2036. <https://doi.org/10.5194/bg-8-2027-2011>
- Roberts, G., Wooster, M., Xu, W., Freeborn, P. H., Morcrette, J. J., Jones, L., et al. (2015). LSA SAF meteosat FRP products-Part 2: Evaluation and demonstration for use in the Copernicus atmosphere monitoring service (CAMS). *Atmospheric Chemistry and Physics*, 15(22), 13241–13267. <https://doi.org/10.5194/acp-15-13241-2015>
- Roy, D. P., & Boschetti, L. (2009). Southern africa validation of the MODIS, L3JRC and GlobCarbon burned area products. *Transactions on Geoscience and Remote Sensing*, 47(4), 1032–1044. <https://doi.org/10.1109/TGRS.2008.2009000>
- Running, S. W., Nemani, R. R., Heinsch, F. A., Zhao, M., Reeves, M., & Hashimoto, H. (2004). A continuous satellite-derived measure of global terrestrial primary production. *BioScience*, 54(6), 547–560. [https://doi.org/10.1641/0006-3568\(2004\)054\[0547:ACSMOG\]2.0.CO;2](https://doi.org/10.1641/0006-3568(2004)054[0547:ACSMOG]2.0.CO;2)
- Seiler, W., & Crutzen, P. J. (1980). Estimates of gross and net fluxes of carbon between the biosphere and the atmosphere from biomass burning. *Climatic Change*, 2(3), 207–247. <https://doi.org/10.1007/bf00137988>
- Shi, Y., Zang, S., Matsunaga, T., & Yamaguchi, Y. (2020). A multi-year and high-resolution inventory of biomass burning emissions in tropical continents from 2001–2017 based on satellite observations. *Journal of Cleaner Production*, 270, 122511. <https://doi.org/10.1016/j.jclepro.2020.122511>
- Smith, W. K., Reed, S. C., Cleveland, C. C., Ballantyne, A. P., Anderegg, W. R. L., Wieder, W. R., et al. (2015). Large divergence of satellite and Earth system model estimates of global terrestrial CO<sub>2</sub> fertilization. *Nature Climate Change*, 6(3), 306–310. <https://doi.org/10.1038/nclimate2879>
- Stocker, B. D., Zscheischler, J., Keenan, T. F., Prentice, I. C., Seneviratne, S. I., & Peñuelas, J. (2019). Drought impacts on terrestrial primary production underestimated by satellite monitoring. *Nature Geoscience*, 12(4), 264–270. <https://doi.org/10.1038/s41561-019-0318-6>
- Syampungani, S., Geldenhuys, C. J., & Chirwa, P. W. (2016). Regeneration dynamics of miombo woodland in response to different anthropogenic disturbances: Forest characterisation for sustainable management. *Agroforestry Systems*, 90(4), 563–576. <https://doi.org/10.1007/s10457-015-9841-7>
- Wooster, M., Roberts, G., Freeborn, P. H., Xu, W., Govaerts, Y., Beeby, R., et al. (2015). LSA SAF Meteosat FRP products-Part 1: Algorithms, product contents, and analysis. *Atmospheric Chemistry and Physics*, 15(22), 13217–13239. <https://doi.org/10.5194/acp-15-13217-2015>
- Zhang, X., Wang, J., Gao, F., Liu, Y., Schaaf, C., Friedl, M., et al. (2017). Exploration of scaling effects on coarse resolution land surface phenology. *Remote Sensing of Environment*, 190, 318–330. <https://doi.org/10.1016/j.rse.2017.01.001>
- Zhao, Z., Li, W., Ciais, P., & Wigneron, J.-P. (2022). Central african biomass carbon loss counterbalanced by carbon gains during 2010–2019. In *AGU fall meeting abstracts* (Vol. 2022, p. B51D-03)